

AMERICAN UNIVERSITY OF BEIRUT

Modeling and Analysis of a Holonomic and
Nonholonomic Novel Differential Drive Wheeled
Robotic System

by
Mohamad Alsalman

A thesis
submitted in partial fulfillment of the requirements
for the degree of Master of Engineering
to the Department of Mechanical Engineering
of the Faculty of Engineering and Architecture
at the American University of Beirut

Beirut, Lebanon
April 2016

AMERICAN UNIVERSITY OF BEIRUT

Modeling and Analysis of a Holonomic and Nonholonomic Novel Differential Drive Wheeled Robotic System


by
Mohamad Alsalman

Approved by:

Dr. Elie Shammass, Assistant Professor


Advisor

Mechanical Engineering


Dr. Daniel Asmar, Associate Professor

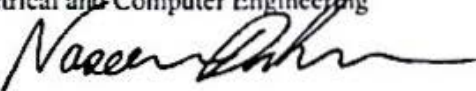
Member of Committee

Mechanical Engineering


Dr. Naseem Daher, Assistant Professor

Member of Committee

Electrical and Computer Engineering



Date of thesis defense: April 22, 2016

AMERICAN UNIVERSITY OF BEIRUT

THESIS, DISSERTATION, PROJECT RELEASE FORM

Student Name: _____
Last First Middle

Master's Thesis Master's Project Doctoral Dissertation

I authorize the American University of Beirut to: (a) reproduce hard or electronic copies of my thesis, dissertation, or project; (b) include such copies in the archives and digital repositories of the University; and (c) make freely available such copies to third parties for research or educational purposes.

I authorize the American University of Beirut, **three years after the date of submitting my thesis, dissertation, or project**, to: (a) reproduce hard or electronic copies of it; (b) include such copies in the archives and digital repositories of the University; and (c) make freely available such copies to third parties for research or educational purposes.

Signature

Date

Acknowledgements

I am extremely thankful and grateful to Dr. Elie Shammas, my supervisor, for his ever present advice and guidance to help me proceed with my work, as well as his support and patience when I faced dead ends and rough patches. His continuous support paved the way for this work and my future, and it goes without saying that this would not be possible without him as my advisor. He always seemed to look for the right questions which needed answering, and I often left the meetings perplexed but with a fuller understanding of the bigger picture.

I am grateful to Dr. Naseem Daher for his guidance, especially when I faced tough problems in control. This work would have taken much more time and effort without his advice.

I am thankful to Dr. Daniel Asmar for his advice and support as a leader in our research group.

An Abstract of the Thesis of

Mohamad Alsalman for Master of Engineering
Major: Mechanical Engineering

Title: Modeling and Analysis of a Holonomic and Nonholonomic Novel Differential Drive Wheeled Robotic System

Modeling and control of wheeled mobile robots over rough terrain has been an essential task for robotic researchers for applications such as search and rescue and unmanned exploratory missions. Modeling the locomotion of a wheeled robot on rough terrain yields a highly constrained system of equations of motion.

This work presents the modeling and control of a variable-diameter differentially-drive robot with a single actuator. The forward motion of this model can be dynamically related to the rotation of a central disk whereas the steering motion of the model can be related to the translation of this disk. The motion of this novel robotic platform design is captured via a set of differential algebraic equations (DAE). In this thesis, a stabilization technique is developed and used to reduce the DAEs of motion to a set of ordinary differential equations. This stabilization method proved to be adequate to model the motion of the platform, not only on flat terrain but also on rugged uneven terrain. The developed model was used to simulate various inputs in an open-loop architecture to analyze the systems motion and its interactions with bumps in the terrain.

A final task was to utilize the developed model to design controllers for the system inputs to perform two tasks, trajectory following and bump or disturbance mitigation. The stabilization of the equations of motion developed in this thesis, proved to be helpful in linearizing the dynamics the system. Accordingly, the linear system was used to analyze the systems controllability as well as to develop a Linear Quadratic Regulator which was tuned to provide robust control for the system.

Contents

Acknowledgements	v
Abstract	vi
List of Figures	x
List of Tables	xi
1 Introduction	1
1.1 Differential Drive and Variable Diameter Wheeled Robots	2
1.2 Wheeled Robots on Uneven Terrain	4
2 Background	6
2.1 Equations of Motion for Mechanical Systems	6
2.1.1 Lagrangian Formulation for the Equations of Motion	9
2.1.2 Rewriting the Equations of Motion in Matrix Form	13
2.2 Differential Algebraic Equations	14
2.2.1 Differential Algebraic Equation Index Reduction	17
2.2.2 Control for Simulation Purposes	23
3 Stabilization, Linearization and Control	25
3.1 Stabilization Methods for Constrained Systems	25
3.1.1 Simulation-Friendly Method to Simplify DAEs	30
3.2 Linearization and Control	31
3.2.1 Linearization	31
3.2.2 Controllability and Decomposition of Uncontrollable Systems	33
3.2.3 The Linear Quadratic Regulator	34
4 Modeling Flexible Wheels	39
4.1 Modeling and Analysis of a Two-Dimensional Flexible Wheel on Flat and Uneven Terrain	39
4.2 Modeling a Three-Dimensional Wheel over Rough Terrain	43
4.3 Bump Analysis	47

5	Modeling, Analysis, and Control	49
5.1	Initial Vehicle Three-Dimensional Modeling, Analysis, and Simulation over Flat Terrain	49
5.1.1	Vehicle over Flat Terrain	49
5.1.2	Path Planning over Flat Terrain	53
5.2	Initial Vehicle Three-Dimensional Modeling, Analysis and Simulation over Rough Terrain	56
5.2.1	Single Inclined Wheel over Rough Terrain	56
5.2.2	Full System over Rough Terrain	58
5.2.3	Simulation and Discussion	61
5.3	Simplified Three-Dimensional Model and Control	65
5.3.1	System Model	65
5.3.2	Control and Simulations	67
6	Conclusion	72
	Bibliography	73

List of Figures

1.1	The designs found in the literature	3
1.2	Designs used to traverse uneven terrain	4
2.1	2 Dimensional Pendulum	7
2.2	The classical rolling disk example	8
2.3	A look at the general equations of motion for constrained mechanical systems	15
2.4	First method to simplify constrained mechanical systems	16
2.5	Second method to simplify constrained mechanical systems	24
3.1	Third method to simplify constrained mechanical systems	29
3.2	Fourth method to simplify constrained mechanical systems	31
3.3	Desired equilibrium trajectory	36
3.4	The torque inputs and resulting rotational velocities for the simulated linear and nonlinear systems	37
3.5	Parametric plots of the $x - y$ position of the vehicle simulated using the linear and nonlinear model	38
4.1	The model for the variable diameter disk	40
4.2	Studying the 2D disk over flat terrain for constant velocity	42
4.3	Single smooth bump used in 2D simulations	42
4.4	Studying the 2D disk over a bump, plotting the radius	43
4.5	3D disk model and coordinates	44
4.6	Gaussian bump model	46
4.7	Results for the 1st bump model	46
4.8	2nd bump model going from 0 to 0.5	47
4.9	Results for 2nd bump model	47
4.10	A static figure showing the disk on a bump	48
5.1	Sfeir's Design	50
5.2	The full vehicle model over flat terrain	51
5.3	Front and top views of the vehicle	52
5.4	Controller Performance	54
5.5	Effects of controlled coordinates on driving coordinate ϕ	55

5.6	The vehicle velocity for the different simulations	55
5.7	Comparison of ideal Dubins path, uncorrected implement path, and corrected implement path.	56
5.8	Single wheel on rough terrain	57
5.9	Two dimensional projection of terrain surface function onto wheel plane	57
5.10	Two wheeled system on rough terrain	58
5.11	The variation of d , $\dot{\alpha}$, and $\dot{\phi}$	62
5.12	The x-y trajectory traversed by the vehicle compared to the actual Dubins path	63
5.13	Simulation results over rough terrain	64
5.14	Initial simulation result for the controlled system following a line trajectory	68
5.15	The relationship between z and β with a disturbance on β	68
5.16	The motion of the controlled system in the x-y plane following a line trajectory with a disturbance on β	69
5.17	The relationship between z and β with disturbances on z and β	69
5.18	The motion of the controlled system in the x-y plane following a line trajectory with disturbances on z and β	69
5.19	Initial simulation result for the controlled system following a circular trajectory	70
5.20	Simulation result for the controlled system following a circular trajectory with a disturbance on the inclination angle	71

List of Tables

5.1	The proposed system parameter and controller gains.	54
5.2	Path errors	55
5.3	The proposed system parameters and controller gains.	62

Chapter 1

Introduction

Mobile robotics is the branch of engineering that deals with the modeling, design, and control of terrain, aerial, and underwater vehicles. These vehicles are designed knowing the restrictions forced upon them by their respective applications and environments. Aerial and underwater vehicles are subjected to great amounts of forces from the air and water currents they traverse, leading engineers into their domain of study. Land vehicles on the other hand are under contact forces from their surroundings, which have provided a very difficult problem for researchers. Motion constraints in robotic locomotion have been thoroughly studied for wheeled platforms moving over flat terrain, but get much more complicated when the robot is allowed to traverse uneven terrain, where a deep analysis and understanding of contact is required. Researchers have often studied the mathematical representations of wheeled systems on rough terrain, most notable the forces due to the wheel contact with the terrain. Enforcing the contact between two bodies has been tackled by researchers from several angles, many of which require a range of sensors, and remain unsatisfactory from a purely dynamic point of view. In addition to the literature dealing with the dynamics involved, some work has been done to design a feasible robotic vehicle that can traverse uneven terrain while satisfying the required constraints. Many researchers tend to use two wheeled differential driven robots, as compared to four or more wheeled vehicles, providing a simpler system to model, with desirable mobility. When simplistic system designs were proven to fail over rough terrain, as the required constraints would no longer be satisfied, research focused on more flexible designs, including variable length axles and stoked designs.

In this work, the problem of designing a feasible system that can traverse flat terrain easily in addition to providing satisfactory rough terrain mobility is addressed. The resulting design is a flexible wheeled vehicle, which was modeled in two and three dimensions by addressing the simple components before combining them. This design is then fully modeled using index reduction techniques to simplify the constrained equations of motion. The path following capabilities of the system are studied, comparing the dynamic motion to Dubins kinematic minimum path approach. The model is then amended to analyze its rough terrain mobility, and the mitigation of bump-like

disturbances.

Some of these previous designs are presented in sections 1.1 and 1.2. This is followed by a full study of dynamic system modeling and analysis in section 2.1, and a study of the mathematical techniques involved in these formulations in section 2.2. Chapter 3 presents the stabilization techniques developed in the literature and the novel method utilized in this work. This method is used to aid in the linearization, decomposition and control of nonlinear systems derived from the Lagrangian formulation. The remainder of this work utilizes this background to model one of the designs in the literature in a unique way. Chapter 4 looks into flexible wheel models and the effect of rough terrain on their parameters in two and three dimensions. Chapter 5 presents the modeling, analysis, and control of the full system model along with simulations and results. In section 5.1, a study of the full system model over flat terrain is presented, with path following simulations. Section 5.2 presents the model for rough terrain mobility and simulation, where the model is simulated to follow a Dubins path as well as mitigating a bump in open loop. In section 5.3, the controller design is discussed for a simpler iteration of the model, where robust control is implemented for disturbance rejection.

1.1 Differential Drive and Variable Diameter Wheeled Robots

In the study of wheeled robots, the search for high mobility, simple design, and minimal actuation has been one of the main concerns of robotic researchers. The literature over the years has tackled all of those concerns, with differential drive being a frequently visited design by many researchers, as seen in Fig.1.1.

O'Halloran and his colleagues [1] designed and tested a high impact survivable robot based on differential drive designs. The use of differential drive was essential because it allowed for a compact build thus the vehicle was able to withstand drops from up 20 feet. Their work conveys the advantage of differential drive in the search of compact and durable builds. Other researchers have found the versatility of differential drive to be of great use, as many novel designs with specified usage have come up in the literature. One of the design trends for differential drive is to use variable diameter wheels where the change in diameter effects a change in the forward velocity of the wheels. Lee et al. [2] combine the ingenuity of the Japanese art of origami with robotics to achieve a differential drive robot using a magic ball origami structure. This structure can take the shape of a long cylindrical tube or a circular one, where the variation in diameter allows the vehicle to describe the dynamics of a differential drive. Some more complicated and highly actuated designs have been tackled as well; Zheng [3] designed a retractable structure that is driven by a central axis, where rotating the axis expands and contracts the outer structure, thus increasing and decreasing the wheel diameter in the process. This design combines the high stability of wheeled

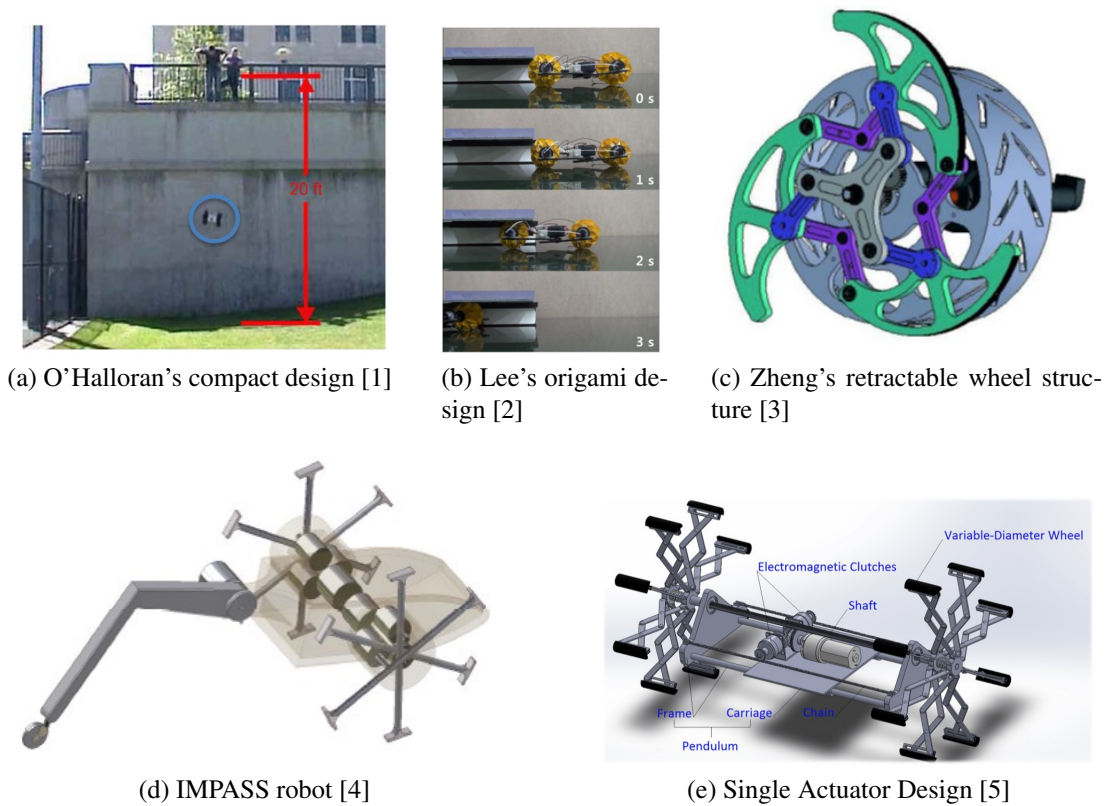


Figure 1.1: The designs found in the literature

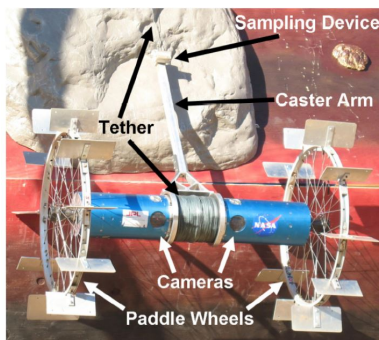
robots with the high mobility of legged robots over uneven terrain, as the retractable structure has shown good performance in obstacle climbing simulations. The IMPASS robot [4], on the other hand, consists of spoked wheels that are individually actuated, allowing for high mobility over rough terrain, in contrast to the high degree of actuation required. The stability of this design is studied as the wheel-ground contact varies based on the desired mode of motion, varying from one contact point up to three contact points. These designs have tackled the problems of compactness with versatility and maneuverability in rough environments, however the actuation of these designs is demanding.

A more recent design by Sfeir [5] looks into minimal actuation with high terrain mobility. Their design consists of a two wheeled variable diameter vehicle with a single actuator, given by a mass on the wheels' axis, that moves along the axis and rotates about it. As the actuator moves along the axis, the wheel diameters increase and decrease based on a spring-damper system installed, and as the actuator rotates about the axis, inertia effects result in a rotation of the whole vehicle, thus inducing the forward motion. This design solves a problem in reduced actuation thus simplifying the design.

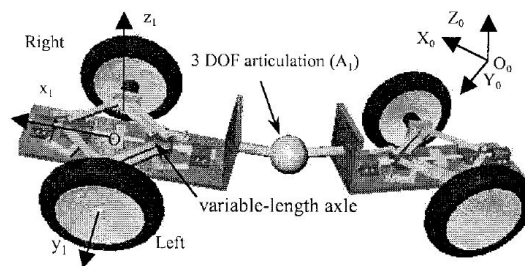
As is the case for all two wheeled robotic systems, these designs are under con-

straints from the environment[6, 7]. For flat terrain, these constraints are the no-skidding constraint along the lateral direction of the vehicle, and the no-slipping constraints along the forward direction of each wheel. However when traversing rough terrain, these constraints are insufficient to model the system.

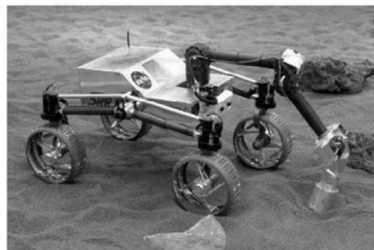
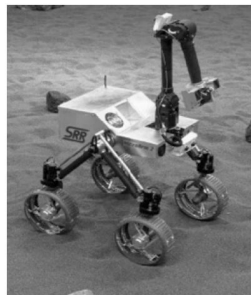
1.2 Wheeled Robots on Uneven Terrain



(a) Axel 1 tethered rover [8]



(b) Choi's design for a variable length axle vehicle [9]



(c) Jet Propulsion Laboratory's Sample Return Rover [10]

Figure 1.2: Designs used to traverse uneven terrain

When traversing uneven terrain, wheeled mechanical systems undergo varied forces and dynamics as compared to flat terrain. The main goal in modeling systems over rough terrain is the maintenance of contact, assuming sufficient smoothness. In much of the literature, point contact between the wheel and the terrain is assumed, thus an additional constraint is required to keep that contact. This type of constraint is seen frequently in the literature as a holonomic constraint, as Choi [9] used a position constraint on the contact of the wheel to satisfy a predefined terrain function, in addition to using an altered version of Baumgarte's nonholonomic stabilization formula [11] to achieve a working model for simulation. Using the holonomic constraint allows researchers to interpret the third spatial coordinate without needing to explicitly calculate it. For vehicles over flat terrain, this constraint is trivial because the models are

basically planar in $x - y$, and the z dimension is seen to be constant or a function of the design. However, over uneven terrain, the vehicle moves in three dimensions, and the wheel-ground contact angles rarely coincide with the world frame's z axis, rather they are tangent to the terrain at the contact point. This fact is used by Cai and Roth to develop some theory of point contact in planar motion [12] as well as spatial motion [13] regarding rigid bodies that remain in contact. In their work, they make use of the geometries of the bodies involved, and utilize the fact that, considering point contacts, the normal lines to the curves at contact should coincide, and the contact point moves in the direction of the common tangent. This analysis brings forth the use of a non-holonomic constraint rather than a holonomic one, which prevents the contact point from moving in the direction normal to the terrain.

Additional work on nonholonomic constraint for traversing rough terrain was done by Choi and Sreenivasan [9, 14]. Aiming to preserve the no-skidding and no-slipping constraints, they define a design requirement for robotic vehicles to be able to traverse uneven terrain, namely $(lc_z - nc_x)(\omega_1 - \omega_2) = 0$, which requires either variable length wheel axles or for the wheels to rotate at the same angular velocity. They show that a vehicle that doesn't satisfy this constraint will undergo slipping when traversing uneven terrain. Leading researchers to the use of actively and passively articulated systems as seen in Fig. 1.2.

Iagnemma et al. [10] use the actively articulated suspension of the Jet Propulsion Lab's Sample Return Rover to traverse uneven terrain. Assuming point contact, they estimate contact angles from sensor measurements, and through the use of the active suspension they ensure stability of the vehicle by finding the optimal configuration for the measured angle values. The use of holonomic constraints for uneven terrain has also been seen in the case of tethered robots where Abad-Manterola [8] and his colleagues develop an algorithm for tethered robot motion on steep terrain, using holonomic constraints to model the tether reaction force as well as the caster arm ground reaction force.

Chapter 2

Background

In this chapter, the Lagrangian formulation is presented for constrained systems, resulting in a set of differential algebraic equations. These equations have a high index and additional index reduction steps are required to reduce the index of the system resulting in ordinary differential equations that are simpler to work with and easier to simulate.

2.1 Equations of Motion for Mechanical Systems

The study of dynamic systems and their classification began with the early theories and methods of Newton to the relatively newer formulations of Euler, Lagrange, and Hamilton. The work of these great minds has kept researchers busy, with their work being a cornerstone for many academics in physics and engineering. To progress in the study of dynamic systems, some concepts of classical mechanics are described here, epitomized by the Lagrangian formulation, and reaching the Euler-Lagrange equations of motion.

A mechanical system is characterized as consisting of N particles, such that a particle is defined as a point in space with a given mass. The motion of each such particle is thus defined as a motion of a point in space, which can be fully described by its set of coordinates q , assuming the point has no geometrical dimensions and thus no orientation. Consequently a mechanical system with N particles is said to have Nq *generalized coordinates* that fully describe the motion of the system. This characteristic is to be distinguished from the system's degrees of freedom because a system might require Nq coordinates to be fully defined, but its motion might not be free in all these coordinates. The number of degrees of freedom of a system can be interpreted as the number of *independent* quantities that must be specified to define the system [15].

Some systems in space are not simply defined as points, but a set of points connected by links. This type of system is called a rigid body. When looking into the dynamics of rigid bodies rather than points, spatial coordinates are insufficient to define the system because a system with dimensions, *i.e.* consists of several points connected

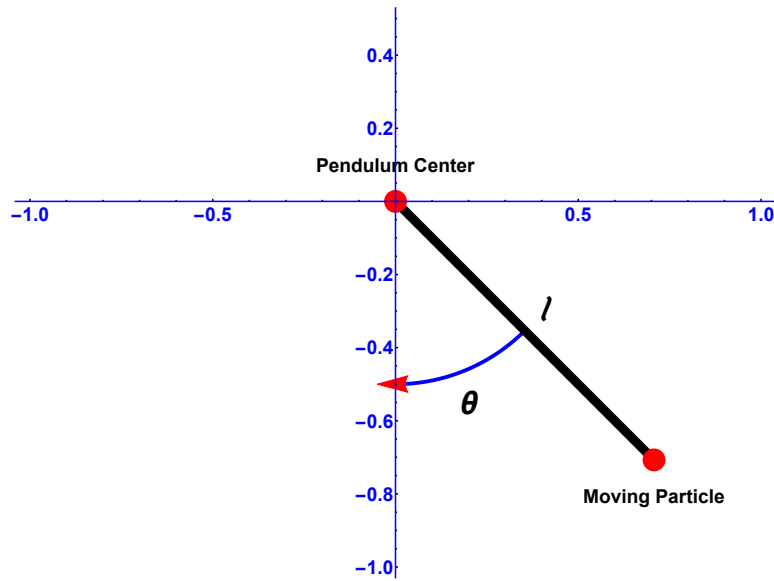


Figure 2.1: 2 Dimensional Pendulum

by links, has an orientation, and this orientation is required to define the motion of the body. An example of this is seen for a rigid body in 3D space, where a point only requires 3 coordinates (x, y, z) to be fully defined, a body requires 6 coordinates which include the spatial coordinates in addition to the 3 rotational coordinates, commonly referred to as roll, pitch and yaw.

Example 1 Consider a system of a pendulum in 2D space, which is basically a particle with coordinates (x, y) allowed to move while remaining at a constant distance from another stationary point in space, the center of the pendulum. The set of coordinates needed to define this pendulum is

$$q = (x, y). \quad (2.1)$$

If the particle is allowed to move freely, the system is said to have 2 degrees of freedom, but a pendulum, in fact, has 1 degree of freedom because it rotates around a fixed center point.

Example 2 A system frequently referred to in dynamics is the rolling disk in a plane seen in Fig.2.2. The disk is allowed to move over the plane but not in the third dimension, so the spatial coordinates (x, y) are required. It is also oriented in a certain direction in the plane so that that direction θ is required. Finally, the motion of the disk is caused by its rolling about its axis, labeled ϕ , and is required to fully define the motion of the system resulting in the set

$$q = (x, y, \theta, \phi). \quad (2.2)$$

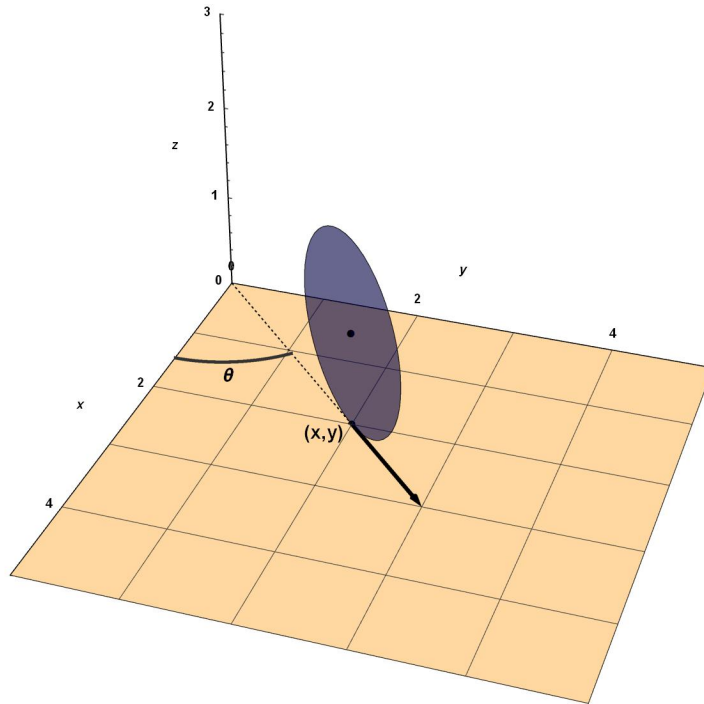


Figure 2.2: The classical rolling disk example

Classifying dynamic systems as constrained or unconstrained, constrained systems can then be studied thoroughly, where the unconstrained systems are a simpler set of the more general formulations. Constrained systems are classified into *holonomic* and *nonholonomic* systems, having *holonomic* and *nonholonomic* constraints, respectively. Both types of constraints have been studied extensively since the beginning of the domain of classical dynamics. Holonomic constraints, similar to the pendulum constraint mentioned earlier, are constraints that take the form

$$\phi_j(q_1, q_2, \dots, q_n) = 0, \quad (j = 1, 2, \dots, k) \quad (2.3)$$

where k is the number of constraints, and q_1, \dots, q_n are the generalized coordinates of the system. The constraints in equation (2.3) are position-level constraints such as length constraints, *i.e.* strictly functions of the generalized coordinates, and in general are called integrable.

Nonholonomic constraints, also termed nonintegrable, take the form of

$$\sum_{i=1}^n a_{ji} dq_i = 0, \quad (j = 1, 2, \dots, m) \quad (2.4)$$

where one can see that these constraint are velocity-level constraints, and cannot be integrated to obtain direct position-level equivalents.

Example 1 Revisited The pendulum mentioned earlier was said to have 1 degree of freedom, despite the point on its end describing a trajectory in 2 dimensions (x, y) . This

constraint is a holonomic constraints portraying the rigidity of the pendulum, *i.e.* the link joining the fixed center point and the moving point being at a constant distance. This constraint is written as

$$x^2 + y^2 - l^2 = 0. \quad (2.5)$$

Note One can see that the pendulum system can be simplified by taking one coordinate θ which is sufficient to define the system. The moving point coordinates can then be defined as $(l \cos \theta, l \sin \theta)$ and the constraint is implicit in this definition. In this text, the coordinates (x, y) will be used instead to portray concepts on constraints and differential equations seen later.

Example 2 Revisited A common example of nonholonomic constraints is that of a disk rolling without slipping on a horizontal plane, mentioned earlier in Fig.2.2. Where the contact point is constrained to have velocity $V_{contact} = r\dot{\phi}$, the following constraint equations can be identified

$$\begin{aligned} \dot{x} - r \cos(\theta) \dot{\phi} &= 0, \\ \dot{y} - r \sin(\theta) \dot{\phi} &= 0, \end{aligned} \quad (2.6)$$

where the velocity of the wheel in the global x and y directions are constrained to be the rotation of the wheel multiplied by its radius, then projected on the appropriate axis. In many cases this constraint is taken in a local body frame of the disk, and in such cases the velocity in the direction of the body y frame, usually taken to be the lateral axis, is taken to be 0, and in the x frame to be simply $r\dot{\phi}$.

When solving for the equations of motion of a classical dynamic system, two approaches are commonly used, vectorial dynamics and analytical dynamics. Vectorial dynamics relies on a complete understanding of the forces and motions within the system, as it applies directly on Newton's laws. Analytical dynamics, on the other hand, is *energy based* and studies a dynamic system as a whole looking into its kinetic and potential energies. Analytical dynamics is based around the Lagrangian formulation, and excels in more complicated constrained systems compared to vectorial dynamics where a complete and thorough understanding of all the forces acting on the system is required [16].

2.1.1 Lagrangian Formulation for the Equations of Motion

Consider a system of N particles described by the generalized coordinates q_1, q_2, \dots, q_s . The principle of least action, also known as Hamilton's principle, states that the system is characterized by a function $L(q_1, q_2, \dots, q_s, \dot{q}_1, \dot{q}_2, \dots, \dot{q}_s, t)$ or $L(q, \dot{q}, t)$ such that the motion of the system satisfies a certain condition. Considering that a certain system occupies, at time t_1 a coordinate q^1 and at time t_2 a coordinate q^2 , this condition states

that the system moves from q^1 to q^2 with the integral

$$\int_{t_1}^{t_2} L(q, \dot{q}, t) dt, \quad (2.7)$$

taking the least possible value. Here we call the function L the **Lagrangian** of the system. The Lagrangian here is defined only as a function of q and \dot{q} because a state of a mechanical system at any time t is fully defined with its generalized positions and velocities. It follows that to minimize the integral the following equation must be satisfied

$$\frac{d}{dt} \frac{\partial L}{\partial \dot{q}} - \frac{\partial L}{\partial q} = 0. \quad (2.8)$$

This set of equations is called the Euler-Lagrange set of equations of motion. The quantity termed the Lagrangian in the above formulation must be a quantity that describes any dynamic system in addition to relating the generalized position and the generalized velocities. This quantity turns out to be a measure of energy of the system. To be able to fully define this quantity, we introduce the *ingredients* needed to define our system.

The set of generalized coordinates of the dynamic system is first used to define the energy in the system, with the kinetic energy T being

$$T = \frac{1}{2} \sum_{i=1}^s m_i \left(\sum_{j=1}^n \frac{\partial x_i}{\partial q_j} \dot{q}_j + \frac{\partial x_i}{\partial t} \right)^2, \quad (2.9)$$

while the potential energy U can take the form of energy derived from any number of natural forces, including gravity, electromagnetism, and spring stiffness [15]. Defining the energy in the system, we can compute the Lagrangian

$$L = T - U. \quad (2.10)$$

Systems containing external forces not derivable from the potential energy require an additional term, symbol τ , to account for this force [16]

$$\frac{d}{dt} \frac{\partial L}{\partial \dot{q}_i} - \frac{\partial L}{\partial q_i} = \tau_i. \quad (2.11)$$

For constrained systems, the constraint forces are calculated and plugged into the equations also on the right hand side. In the case of nonholonomic systems with constraints of the form (2.4), the constraint forces can be written in the form

$$c_i = \sum_{j=1}^m \lambda_j a_{ji}, \quad (i = 1, 2, \dots, n) \quad (2.12)$$

where λ are called Lagrange multipliers. The resulting equations of motion will thus be [16]

$$\frac{d}{dt} \frac{\partial L}{\partial \dot{q}_i} - \frac{\partial L}{\partial q_i} = \tau_i + \sum_{j=1}^m \lambda_j a_{ji}. \quad (2.13)$$

In the case of holonomic constraints of the form (2.3), the constraints forces can be introduced into the system in one of two ways. The first is similar to nonholonomic forces. The constraints are first written as

$$\sum_{i=1}^n b_{ji}q_i = 0, \quad (j = 1, 2, \dots, k) \quad (2.14)$$

and thus the constraint forces can be found to be

$$h_i = \sum_{j=1}^k \lambda_j b_{ji}, \quad (i = 1, 2, \dots, n) \quad (2.15)$$

similar to the forces for nonholonomic systems.

$$\frac{d}{dt} \frac{\partial L}{\partial \dot{q}_i} - \frac{\partial L}{\partial q_i} = \tau_i + \sum_{j=1}^m \lambda_j b_{ji}. \quad (2.16)$$

The other way is to add the constraints straight into the Lagrangian of the system to obtain a new Lagrangian as

$$L' = L + \lambda_j \phi_j(q_i) = L + \sum_{j=1}^k \lambda_j b_{ji} q_i, \quad (i = 1, 2, \dots, n) \quad (2.17)$$

where λ_j are added to the set of generalized coordinates, and the constraint forces appear in the Euler Lagrange equations for $q_i \neq \lambda_j$, and the constraint equations themselves appear for $q_i = \lambda_j$.

Some dynamic systems are under forces that cannot be taken under constraint forces nor generalized forces, they are forces due to dissipation effects, specifically damping components in the system. These forces take the form

$$Q_i = - \sum_{j=1}^n c_{ij}(q, t) \dot{q}_j, \quad (2.18)$$

where $c_{i,j}$ are known as the damping coefficients. These dissipative forces result in energy loss of the system. To introduce them into the Euler Lagrange equations, we define Rayleigh's dissipation function

$$F = \frac{1}{2} \sum_{i=1}^n \sum_{j=1}^n c_{ij} \dot{q}_i \dot{q}_j, \quad (2.19)$$

and the Euler Lagrange equations become

$$\frac{d}{dt} \frac{\partial L}{\partial \dot{q}_i} - \frac{\partial L}{\partial q_i} + \frac{\partial F}{\partial \dot{q}_i} = 0. \quad (2.20)$$

Generalizing all the terms that can go into the Euler-Lagrange equations, we get the following general form to be used, appended by the constraint equations

$$\begin{aligned} \frac{d}{dt} \frac{\partial L}{\partial \dot{q}_i} - \frac{\partial L}{\partial q_i} + \frac{\partial F}{\partial \dot{q}_i} &= \tau_i + \sum_{j=1}^m \lambda_j a_{ji} + \sum_{k=1}^n \lambda_k b_{ki}, \\ \sum_{i=1}^n a_{ji} dq_i + a_{jt} dt &= 0, \\ \phi_j(q_1, q_2, \dots, q_n, t) &= 0. \end{aligned} \quad (2.21)$$

Example 1 In the case of the pendulum, we define our set of generalized coordinates $q = (x, y)$ being the position of the moving point. We can define the energy on the system as

$$\begin{aligned} T &= \frac{1}{2} m \dot{q} \cdot \dot{q} = \frac{1}{2} m (\dot{x}^2 + \dot{y}^2), \\ U &= mgy, \end{aligned} \quad (2.22)$$

where m and g are the mass of the particle and the gravitational constant, respectively. The constraint on the system is

$$x^2 + y^2 - l^2 = 0, \quad (2.23)$$

where l is the length of the rod. The equations of motion are thus

$$\begin{aligned} m\ddot{x} &= \tau_x + 2x\lambda, \\ m\ddot{y} + mg &= \tau_y + 2y\lambda, \\ x^2 + y^2 - l^2 &= 0. \end{aligned} \quad (2.24)$$

Example 2 For the case of the nonholonomic disk, given the set of generalized coordinates (x, y, θ, ϕ) , we can define the center of mass of the disk as the center point, given the coordinates (x, y) with a mass m and moments of inertia J_θ and J_ϕ . The energy in this system is thus

$$T = \frac{1}{2} m (\dot{x}^2 + \dot{y}^2) + \frac{1}{2} J_\theta \dot{\theta}^2 + \frac{1}{2} J_\phi \dot{\phi}^2, \quad (2.25)$$

where the potential energy is always zero as the disk is always on the same level. The nonholonomic constraints repeated here

$$\begin{aligned} \dot{x} - r \cos(\theta) \dot{\phi} &= 0, \\ \dot{y} - r \sin(\theta) \dot{\phi} &= 0, \end{aligned} \quad (2.26)$$

where the matrix a from equation (2.12) is

$$a = \begin{pmatrix} 1 & 0 & 0 & -r \cos \theta \\ 0 & 1 & 0 & -r \sin \theta \end{pmatrix}. \quad (2.27)$$

Finally, the equations of motion are appended by the constraint equations to get the full set required to solve for the system variables (x, y, θ, ϕ) and the Lagrange multipliers (λ_1, λ_2)

$$\begin{aligned}
m\ddot{x} &= \lambda_1 \\
m\ddot{y} &= \lambda_2 \\
J_\theta \ddot{\theta} &= 0 \\
J_\phi \ddot{\phi} &= -r \cos \theta \lambda_1 - r \sin \theta \lambda_2, \\
\dot{x} - r \sin(\theta) \dot{\phi} &= 0, \\
\dot{y} - r \cos(\theta) \dot{\phi} &= 0.
\end{aligned} \tag{2.28}$$

2.1.2 Rewriting the Equations of Motion in Matrix Form

The dynamic equations of motion (2.21) can be written in their standard form by realizing that the terms that multiply \ddot{q} and \dot{q} can be collected, the resulting form is

$$M(q)\ddot{q} + C(q, \dot{q})\dot{q} + g(q) + b(q)\dot{q} = \tau + A_1(q)^T \lambda_1 + A_2(q)^T \lambda_2, \tag{2.29}$$

where M is termed the inertia matrix which contains all mass and inertia terms that multiply the generalized accelerations in the system, C is termed the Coriolis matrix and is the set of Christoffel symbols of the inertia matrix m such that

$$\begin{aligned}
C_{ij} &= \sum_{k=1}^n \Gamma_{ij}^k(q) \dot{q}_k, \\
\Gamma_{ij}^k(q) &= \frac{1}{2} \left(\frac{\partial M_{ij}}{\partial q_k} + \frac{\partial M_{ik}}{\partial q_j} - \frac{\partial M_{kj}}{\partial q_i} \right),
\end{aligned} \tag{2.30}$$

g are the gravitational forces on the system, b represents the dissipation effects, τ is the set of generalized forces, and A_1 and A_2 are the constraint matrices. These equations are appended by a set of nonholonomic and holonomic constraints defined by

$$\begin{aligned}
N(q, \dot{q}) &= 0, \\
H(q) &= 0.
\end{aligned} \tag{2.31}$$

We differentiate equations (2.31) to obtain constraints on \ddot{q}

$$\begin{aligned}
\frac{dN}{dt} &= \frac{\partial N}{\partial \dot{q}} \frac{d\dot{q}}{dt} + \frac{\partial N}{\partial q} \frac{dq}{dt} + \frac{\partial N}{\partial t} = \frac{\partial N}{\partial \dot{q}} \ddot{q} + \frac{\partial N}{\partial q} \dot{q} + \frac{\partial N}{\partial t} = 0, \\
\frac{dH}{dt} &= \frac{\partial H}{\partial q} \frac{dq}{dt} + \frac{\partial H}{\partial t} = \frac{\partial H}{\partial q} \dot{q} + \frac{\partial H}{\partial t} = 0, \\
\frac{d^2H}{dt^2} &= \frac{\partial H}{\partial q} \frac{d\dot{q}}{dt} + \frac{\partial^2 H}{\partial q^2} \dot{q}^2 + \frac{\partial^2 H}{\partial t^2} = \frac{\partial H}{\partial q} \ddot{q} + \frac{\partial^2 H}{\partial q^2} \dot{q}^2 + \frac{\partial^2 H}{\partial t^2} = 0,
\end{aligned} \tag{2.32}$$

where we have differentiated the holonomic constraints twice and the nonholonomic constraint once, to get constraints on the accelerations of the system. Recognizing that

we can solve for \ddot{q} from (2.29), we replace their solutions in (2.32) and solve for λ_1 and λ_2 , which we can plug back into (2.29) to get a system of equations without the constraints. For solely nonholonomic systems, this has been used very frequently, with the resulting general form for the equations being [17]

$$(\mathbb{I} - A^T(AM^{-1}A^T)^{-1}AM^{-1})(M\ddot{q} + C\dot{q} + g - u) = 0, \quad (2.33)$$

where A is the constraint matrix in Pfaffian form such that the nonholonomic constraints are defined as $A^T\dot{q} = 0$.

This method can sometimes be problematic as the initial constraint of the system is not always satisfied. It can be argued that with the proper initial conditions, considering that $A_1\dot{q} = 0$ and $A_2q = 0$ at the initial state of the system, and satisfying $\dot{A}_1\dot{q} + A_1\ddot{q} = 0$ and $\ddot{A}_2q + 2\dot{A}_2\dot{q} + A_2\ddot{q} = 0$ at all consecutive times would satisfy the initial constraints. Numerical simulations on the other hand do not guarantee this, as numerical solvers are not always error-free, and considering that a small error might dissatisfy the differentiated constraints at some time step, then the error in the initial constraints will increase continuously.

2.2 Differential Algebraic Equations

The constrained equations of motion are a set of differential algebraic equations (DAEs) that seldom have an analytical solution and must be solved numerically. Computer numerical simulation often drifts from the stable values, resulting in compounding erroneous values. To see the effect that this drift might have, assume a holonomic constraint $C = 0$ needs to be satisfied at all times, after a certain period of time t , C drifts to a small value δ , with \dot{C} also drifting to a small value ε . After some time, the error on the constraint increases as it takes the form $C = \varepsilon t + \delta$. The difficulty that numerical simulation poses has led to studies on DAEs and ways to simplify such systems.

The general form of nonlinear differential equations is

$$F(\dot{y}, y, t) = 0, \quad (2.34)$$

where $y(t) \in \mathbb{R} \rightarrow \mathbb{R}^n$ and $F \in \mathbb{R}^n \times \mathbb{R}^n \times \mathbb{R} \rightarrow \mathbb{R}^n$. The set F of differential equations are called implicit ODEs if the Jacobian $\partial F / \partial \dot{y}$ is nonsingular, *i.e.* all variables y have at least one instance of \dot{y} in the set of equations then the system has an index of 0. If $\partial F / \partial \dot{y}$ is singular, then at least one variable y in the equations is algebraic or its time derivative cannot be computed, and the system is labeled as a differential algebraic system of equations.

The difficulty of working with DAEs is mainly due to the high index of the system as defined below.

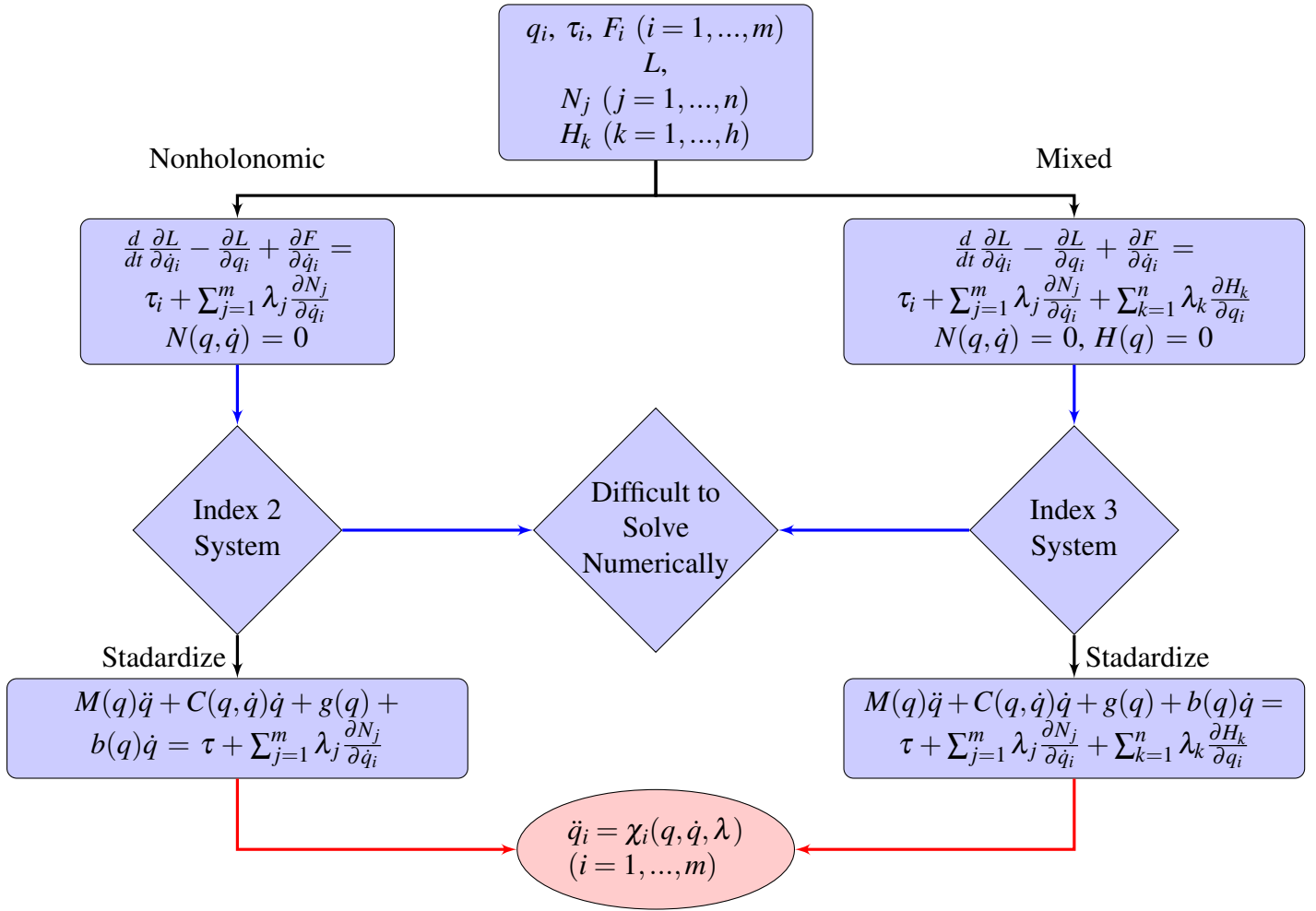


Figure 2.3: A look at the general equations of motion for constrained mechanical systems

Consider a system of equations with an index $i > 0$

$$\begin{aligned}
 F(\dot{y}, y, t) &= 0, \\
 \frac{dF}{dt} &= \frac{\partial F}{\partial \dot{y}} \ddot{y} + \frac{\partial F}{\partial y} \dot{y} + \frac{\partial F}{\partial t} = 0, \\
 \frac{d^2 F}{dt^2} &= \frac{\partial F}{\partial \dot{y}} y^{(3)} + \dots = 0, \\
 &\vdots \\
 \frac{d^s F}{dt^s} &= \frac{\partial F}{\partial \dot{y}} y^{(s+1)} + \dots = 0,
 \end{aligned} \tag{2.35}$$

where the variables $\dot{y}, \ddot{y}, \dots, y^{(s+1)}$ can be considered independent variables and solved for as functions of y and t . It might not be possible to solve for $y^{(s+1)}$, but if it is

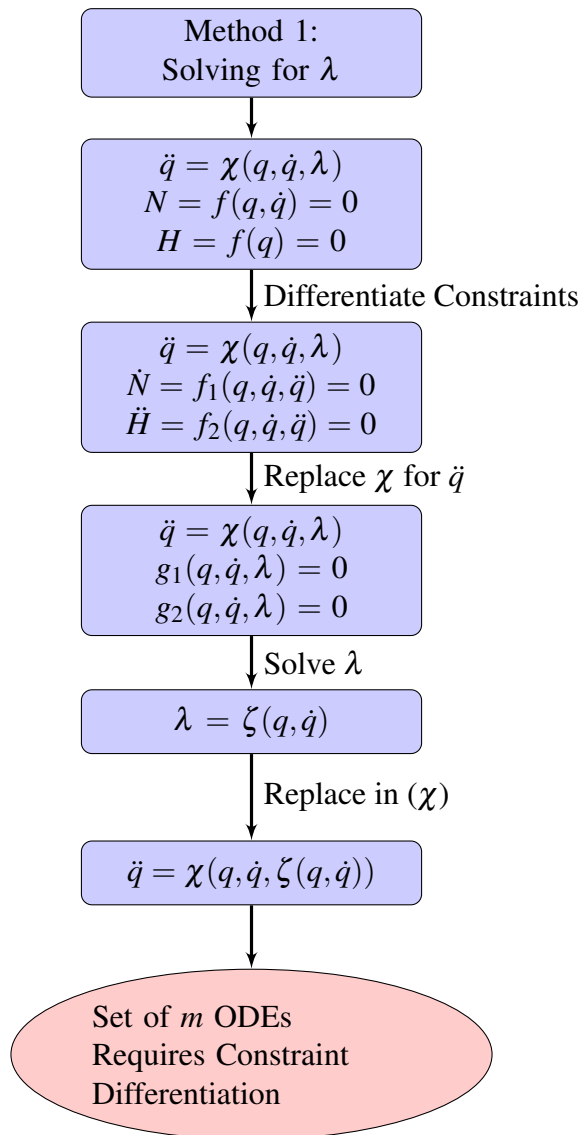


Figure 2.4: First method to simplify constrained mechanical systems

possible to solve for \dot{y} for some value of s , then the index i is defined as the smallest s for which all values \dot{y} can be solved for. One can infer from the system (2.35) that after each differentiation, the index of the system is reduced by one, this is deceiving as the differentiated system does not always convey the same information as the original. This is due to *hidden* constraints within the system, that are lost after each differentiation.

2.2.1 Differential Algebraic Equation Index Reduction

The *general* form of a DAE shown in (2.34) can be transformed into its *semi-explicit* form by replacing \dot{y} with v and y with u to get the system

$$\begin{aligned}\dot{u} &= v, \\ F(v, u, t) &= 0.\end{aligned}\tag{2.36}$$

The index of (2.36) is said to be one more than the general form because an extra differentiation is required to get \dot{v} . This gives insight into index reduction of systems of the form (2.36), or in other words, constrained systems

$$\begin{aligned}\dot{u} - f(u, v, t) &= 0, \\ c(u, v, t) &= 0.\end{aligned}\tag{2.37}$$

The system characterized by (2.37) can be transformed to the general form by replacing v with \dot{y} , where it requires one less differentiation to reach \dot{y} . This index reduction using the general form motivates the study of the *minimum index equivalent* of a system.

An n -dimensional system with index $m > 0$ can be transformed to the minimum index equivalent if for every $i \in n$ where $\partial f / \partial \dot{y}_i = 0$, y is replaced by \dot{y} . This minimum index equivalent can be quite useful for constrained systems as the Lagrange multipliers will typically satisfy $\partial f / \partial \dot{y}_i = 0$. The concept of Lagrange multipliers and index reduction are closely related [18]. Consider a system of the form (2.37), differentiating the constraint gives

$$\frac{\partial c}{\partial u} f(u, v, t) + \frac{\partial c}{\partial v} \dot{v} + \frac{\partial c}{\partial t} = 0,\tag{2.38}$$

where the index of the system has been reduced, except the constraint is essentially different. One can use both constraints, but the system is then overdetermined, so additional variables can be introduced into the system to remove this overdeterminacy.

The following procedure developed by Gear [19] differentiates systems of the general form (2.34) to achieve an index one system, for which many numerical methods exist and provide accurate solutions.

Beginning with a DAE of index $i > 0$ and dimension n_1 , by definition the Jacobian $\partial F / \partial \dot{y}$ is singular, thus has rank $r_1 < n_1$. By the implicit function theorem, one can solve for r_1 variables of the system using the set of r_1 equations that are independent, thus allowing for the change of variable $y = (y_1^T, v_1^T)^T$ where y_1 has r_1 components,

and v_1 represent the remaining unsolved set. We can see that this change of variable allows us to get

$$\dot{y}_1 - e_1(y_1, v_1, \dot{v}_1, t) = 0, \quad (2.39)$$

which can be substituted into the remaining $n_1 - r_1$ equations to get a relationship between y_1 , v_1 , and t . These equations can be interpreted as constraints of the form

$$c_1(y_1, v_1, t) = 0, \quad (2.40)$$

and can be subsequently differentiated to get

$$\frac{\partial c_1}{\partial y_1} e_1(y_1, v_1, \dot{v}_1, t) + \frac{\partial c_1}{\partial v_1} \dot{v}_1 + \frac{\partial c_1}{\partial t} = 0, \quad (2.41)$$

where this new system has a dimension n_2 , where r_2 is the rank of the Jacobian $(\frac{\partial g_1}{\partial y_1} \frac{\partial e_1}{\partial v_1} + \frac{\partial g_1}{\partial v_1})$. Repeating the above step, $v_1 = (y_2^T, v_2^T)^T$ where y_2 has r_2 elements which we can solve for. This process is repeated until the index of the system is fully reduced, specifically i steps, to obtain $\sum_{m=1}^i r_m = n_1$. Finally, we get a set of equations that solves for all the time derivatives of the variables

$$\dot{y} = f(y, t), \quad (2.42)$$

but the system consisting of (2.42) only does not satisfy the same physical phenomena as the original system, because the differentiation leads to a loss of information. The constraints c_1, c_2, \dots, c_i obtained after each differentiation are thus essential to maintain. We write this set of constraints as

$$c(y, t) = 0. \quad (2.43)$$

Simply adding these constraints to the system would make the system overdetermined. To preserve the system determinacy, we introduce the vector μ of the dimension of c and write (2.42) as

$$\dot{y} - f(y, t) - \left(\frac{\partial c}{\partial y}\right)^T \mu = 0, \quad (2.44)$$

which solves the system with the constraints, for $\mu = 0$. The system consisting of (2.43) and (2.44) is an index 2 system because μ can be determined with one differentiation, and $\dot{\mu}$ can thus be determined with 2 differentiations. To reduce the index of the system even further, one has only to notice that μ are strictly algebraic variables, so we can now use the minimal index equivalent of the system and replace the vector $\mu = \dot{c}$ which results in an index one system[18][19]

$$\begin{aligned} \dot{y} &= f(y, t) + \left(\frac{\partial c}{\partial y}\right)^T \dot{v}, \\ c(y, t) &= 0. \end{aligned} \quad (2.45)$$

The system (2.45) is an index 1 system because one differentiation of the 2nd equation gives a solution for \dot{v} . Reducing the system further to index zero is possible but then enforcing the algebraic constraints would not be possible.

Studying the Pendulum Equations In *example 1*, we were able to obtain the equations of motion for the two-dimensional pendulum, repeated below

$$\begin{aligned} m\ddot{x} &= \tau_x + 2x\lambda, \\ m\ddot{y} + mg &= \tau_y + 2y\lambda, \\ x^2 + y^2 - l^2 &= 0. \end{aligned} \quad (2.46)$$

These equations are not of the form (2.34), but can easily be written in that form by a simple change of variable taking $\dot{x} = u$ and $\dot{y} = v$, we obtain the following set of equations

$$\begin{aligned} \dot{x} &= u, \\ \dot{y} &= v, \\ m\dot{u} &= \tau_x + 2x\lambda, \\ m\dot{v} + mg &= \tau_y + 2y\lambda, \\ hc &= x^2 + y^2 - l^2 = 0. \end{aligned} \quad (2.47)$$

We can see that this set of equations, as with all resulting DAE systems from the Euler-Lagrange method that have holonomic constraints, is an index three system[20]. If we differentiate the constraint equations and replace with the appropriate variables we get

$$\begin{aligned} \frac{dhc}{dt} &= xu + yv = 0, \\ \frac{d^2hc}{dt^2} &= -\lambda - y + u^2 + v^2 = 0, \\ \frac{d^3hc}{dt^3} &= -\dot{\lambda} - 3v = 0, \end{aligned} \quad (2.48)$$

where after differentiating three times, we are able to solve for $\dot{\lambda}$. We get the new set of equations

$$\begin{aligned} \dot{x} &= u, \\ \dot{y} &= v, \\ m\dot{u} &= \tau_x + 2x\lambda, \\ m\dot{v} + mg &= \tau_y + 2y\lambda, \\ -\dot{\lambda} - 3v &= 0. \end{aligned} \quad (2.49)$$

But solving the system (2.49) does not represent the solution for system (2.47) because satisfying the differentiated constraint does not ensure that the original constraint is satisfied.

To make sure that all the constraints are satisfied, we distinguish the *hidden* constraint equations that we got from the differentiation

$$\begin{aligned} x^2 + y^2 - l^2 &= 0, \\ xu + yv &= 0, \\ -\lambda - y + u^2 + v^2 &= 0, \end{aligned} \quad (2.50)$$

which define our set c . Adding these constraints immediately to our system makes the system overdetermined, so we define the matrix

$$\frac{\partial c}{\partial y} = \begin{pmatrix} 2x & 2y & 0 & 0 & 0 \\ u & v & x & y & 0 \\ 0 & -1 & 2u & 2v & -1 \end{pmatrix}. \quad (2.51)$$

and introduce the vector μ , which gets rid of the overdeterminacy in the system. The new set of equations is thus

$$\begin{aligned} \dot{x} &= u + 2x\mu_1 + u\mu_2, \\ \dot{y} &= v + 2y\mu_1 + v\mu_2 - \mu_3, \\ m\dot{u} &= \tau_x + 2x\lambda + x\mu_2 + 2u\mu_3, \\ m\dot{v} + mg &= \tau_y + 2y\lambda + y\mu_2 + 2v\mu_3, \\ \dot{\lambda} &= -3v - \mu_3, \\ x^2 + y^2 - l^2 &= 0, \\ xu + yv &= 0, \\ -\lambda - y + u^2 + v^2 &= 0, \end{aligned} \quad (2.52)$$

where we have reduced the index of (2.46) from 3 to 2. We can reduce the system (2.52) further by distinguishing its minimum index equivalent, and introducing the variable $\dot{v} = \mu$. Where the final system will be of index 1.

Studying the Disk Equations In the case of the nonholonomic disk, the equations differ due to the velocity components appearing in the constraint equations, which produce an index 2 system rather than an index 3 system. Looking into the equations of motion seen in (2.28), after changing the variables to account for accelerations

$$\begin{aligned} \dot{x} &= u, \\ \dot{y} &= v, \\ \dot{\theta} &= \omega_1, \\ \dot{\phi} &= \omega_2, \\ m\dot{u} &= \lambda_1 \\ m\dot{v} &= \lambda_2 \\ J_\theta \dot{\omega}_1 &= 0 \\ J_\phi \dot{\omega}_2 &= -r \cos \theta \lambda_1 - r \sin \theta \lambda_2, \\ nhc_1 &= u - r \sin(\theta) \omega_2 = 0, \\ nhc_2 &= v - r \cos(\theta) \omega_2 = 0, \end{aligned} \quad (2.53)$$

where differentiating the constraint equations seen in (2.53) twice gives the re-

quired equations of $\dot{\lambda}_1$ and $\dot{\lambda}_2$

$$\begin{aligned}
\frac{dnhc_1}{dt} &= \frac{r^2 \cos^2(\theta) (\lambda_2 \tan(\theta) + \lambda_1)}{J_2} + \frac{\lambda_1}{m} + r\omega_1 \omega_2 \sin(\theta) = 0, \\
\frac{dnhc_2}{dt} &= \frac{\lambda_2 (-J_2 - mr^2 \sin(\theta)(\sin(\theta) + \cos(\theta))) + J_2 mr \omega_1 \omega_2 \cos(\theta)}{J_2 m} = 0, \\
\frac{d^2nhc_1}{dt^2} &= -\frac{3\lambda_1 r^2 \omega_1 \sin(2\theta)}{J_2} + \frac{3\lambda_2 r^2 \omega_1 \cos(2\theta)}{J_2} + \frac{r^2 \sin(2\theta) \dot{\lambda}_2}{J_2} \\
&+ \frac{r^2 \cos(2\theta) \dot{\lambda}_1}{J_2} - \frac{\lambda_2 r^2 \omega_1}{J_2} + \frac{r^2 \dot{\lambda}_1}{J_2} + \frac{2\dot{\lambda}_1}{m} + 2r\omega_1^2 \omega_2 \cos(\theta) = 0, \\
\frac{d^2nhc_2}{dt^2} &= \frac{3\lambda_2 r^2 \omega_1 \sin(2\theta)}{J_2} + \frac{3\lambda_1 r^2 \omega_1 \cos(2\theta)}{J_2} + \frac{2r^2 \sin^2(\theta) \lambda_2'}{J_2} \\
&+ \frac{r^2 \sin(2\theta) \lambda_1'}{J_2} + \frac{\lambda_1 r^2 \omega_1}{J_2} + \frac{2\lambda_2'}{m} + 2r\omega_1^2 \omega_2 \sin(\theta) = 0.
\end{aligned} \tag{2.54}$$

The system with the twice differentiated constraints is thus

$$\begin{aligned}
\dot{x} &= u, \\
\dot{y} &= v, \\
\dot{\theta} &= \omega_1, \\
\dot{\phi} &= \omega_2, \\
m\dot{u} &= \lambda_1 \\
m\dot{v} &= \lambda_2 \\
J_\theta \dot{\omega}_1 &= 0 \\
J_\phi \dot{\omega}_2 &= -r \cos \theta \lambda_1 - r \sin \theta \lambda_2, \\
\frac{d^2nhc_1}{dt^2} &= -\frac{3\lambda_1 r^2 \omega_1 \sin(2\theta)}{J_2} + \frac{3\lambda_2 r^2 \omega_1 \cos(2\theta)}{J_2} + \frac{r^2 \sin(2\theta) \dot{\lambda}_2}{J_2} \\
&+ \frac{r^2 \cos(2\theta) \dot{\lambda}_1}{J_2} - \frac{\lambda_2 r^2 \omega_1}{J_2} + \frac{r^2 \dot{\lambda}_1}{J_2} + \frac{2\dot{\lambda}_1}{m} + 2r\omega_1^2 \omega_2 \cos(\theta) = 0, \\
\frac{d^2nhc_2}{dt^2} &= \frac{3\lambda_2 r^2 \omega_1 \sin(2\theta)}{J_2} + \frac{3\lambda_1 r^2 \omega_1 \cos(2\theta)}{J_2} + \frac{2r^2 \sin^2(\theta) \lambda_2'}{J_2} \\
&+ \frac{r^2 \sin(2\theta) \lambda_1'}{J_2} + \frac{\lambda_1 r^2 \omega_1}{J_2} + \frac{2\lambda_2'}{m} + 2r\omega_1^2 \omega_2 \sin(\theta) = 0.
\end{aligned} \tag{2.55}$$

The *hidden* constraints c , found to be

$$\begin{aligned}
u - r \sin(\theta) \omega_2 &= 0, \\
v - r \cos(\theta) \omega_2 &= 0, \\
\frac{r^2 \cos^2(\theta) (\lambda_2 \tan(\theta) + \lambda_1)}{J_2} + \frac{\lambda_1}{m} + r \omega_1 \omega_2 \sin(\theta) &= 0, \\
\frac{\lambda_2 (-J_2 - m r^2 \sin(\theta) (\sin(\theta) + \cos(\theta))) + J_2 m r \omega_1 \omega_2 \cos(\theta)}{J_2 m} &= 0,
\end{aligned} \tag{2.56}$$

need to be accounted for by adding the set of multipliers μ and plugging them into the equations as in the previous example.

$$\begin{aligned}
u &= x', \\
v &= y', \\
\omega_1 &= \theta' - \frac{\lambda_1 \mu_3 r^2 \sin(2\theta)}{J_2} + \frac{\lambda_2 \mu_4 r^2 \sin(2\theta)}{J_2} + \frac{\lambda_2 \mu_3 r^2 \cos(2\theta)}{J_2} \\
&+ \frac{\lambda_1 \mu_4 r^2 \cos(2\theta)}{J_2} + \mu_1 r \omega_2 \sin(\theta) + \mu_4 r \omega_1 \omega_2 \sin(\theta) - \mu_2 r \omega_2 \cos(\theta) + \mu_3 r \omega_1 \omega_2 \cos(\theta), \\
\omega_2 &= \phi', \\
\lambda_1 &= \mu_1 + m u', \\
\lambda_2 &= \mu_2 + m v', \\
\mu_3 r \omega_2 \sin(\theta) - \mu_4 r \omega_2 \cos(\theta) &= J_1 \omega_1', \\
J_2 \omega_2' + \lambda_2 r \sin(\theta) + \lambda_1 r \cos(\theta) - \mu_3 r \omega_1 \sin(\theta) \\
+ \mu_4 r \omega_1 \cos(\theta) + \mu_2 r \sin(\theta) + \mu_1 r \cos(\theta) &= 0, \\
-\frac{6\lambda_1 r^2 \omega_1 \sin(2\theta)}{J_2} + \frac{6\lambda_2 r^2 \omega_1 \cos(2\theta)}{J_2} + \frac{2r^2 \sin(2\theta) \lambda_2'}{J_2} + \frac{2r^2 \cos(2\theta) \lambda_1'}{J_2} \\
- \frac{\mu_4 r^2 \sin(2\theta)}{J_2} - \frac{2\mu_3 r^2 \cos^2(\theta)}{J_2} - \frac{2\lambda_2 r^2 \omega_1}{J_2} \\
+ \frac{2r^2 \lambda_1'}{J_2} + \frac{4\lambda_1'}{m} - \frac{2\mu_3}{m} + 4r \omega_1^2 \omega_2 \cos(\theta) &= 0, \\
-\frac{\lambda_2 r^2 \omega_1 \sin(2\theta)}{J_2} - \frac{\lambda_1 r^2 \omega_1 \cos(2\theta)}{J_2} + \frac{2r^2 \sin^2(\theta) \lambda_2'}{J_2} + \frac{r^2 \sin(2\theta) \lambda_1'}{J_2} \\
- \frac{\mu_4 r^2 \sin^2(\theta)}{J_2} - \frac{\mu_3 r^2 \sin(\theta) \cos(\theta)}{J_2} \\
- \frac{3\lambda_1 r^2 \omega_1}{J_2} + \frac{2\lambda_2'}{m} - \frac{\mu_4}{m} + 2r \omega_1^2 \omega_2 \sin(\theta) &= 0.
\end{aligned} \tag{2.57}$$

We can see that the index of the system remains 2, because that's the case initially for nonholonomic systems, and we still need 2 differentiations to get $\dot{\mu}$. To reduce this

system to index 1, we introduce $\dot{v} = \mu$, where one differentiation of the final equations gives the solution for \dot{v} .

These two examples show that index reduction is a very complicated method to simplify higher index DAEs. In dynamic systems, especially, it is very important to satisfy a system's initial constraints at all times in numerical simulations. Providing satisfactory constrained models that are solvable in simulation is a tough task, but Bamgarte shows that it is possible through stabilization methods.

2.2.2 Control for Simulation Purposes

Some steps taken in the index reduction method have brought up the potential usefulness of defining velocity variables such as $u = \dot{x}$, $v = \dot{y}$ and $\omega = \dot{\phi}$. In some system simulations, satisfaction of the velocity is more essential than the position on the control level. This change of variable allows the application of a controller directly on the velocity rather than the position.

In typical dynamic systems, the generalized forces τ_i are the controlling forces and they are made functions of the generalized coordinates so as to satisfy a certain criterion. A frequently used controller in such systems is a P-D controller defined by the equation [21]

$$\tau_i = \ddot{q}_{desired} + K_d(\dot{q}_{desired} - \dot{q}) + K_p(q_{desired} - q), \quad (2.58)$$

where a precise choice of K_d and K_p is required to satisfy our desired q .

A slight variation of this controller is made possible by the introduced variables replacing \dot{q} , where a more robust PID controller can be placed on \dot{q} . Taking $\rho = \dot{q}$, the control law is defined by

$$\tau_i = K_d(\dot{\rho}_{desired} - \rho) + K_p(\rho_{desired} - \rho) + K_i(q_{desired} - q). \quad (2.59)$$

For the purposes of studying the effects of the generalized velocities, this controller has proven to be more robust in the simulations, on the other hand, for position level precision, it doesn't provide the same accuracy.

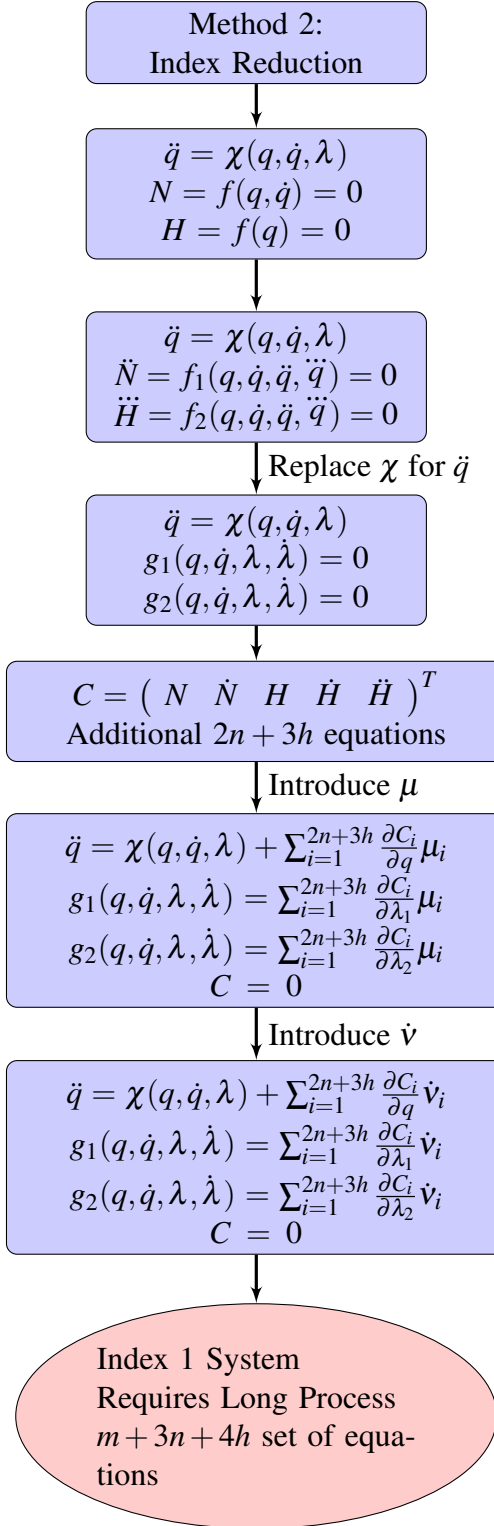


Figure 2.5: Second method to simplify constrained mechanical systems

Chapter 3

Stabilization, Linearization and Control

In this chapter, the stabilization method found in the literature is introduced and improved on using the notion of the minimum index equivalent of the system. This improved stabilization technique was later used for the linearization and control of dynamic equations of motion.

3.1 Stabilization Methods for Constrained Systems

It has been established that differentiation can reduce the index of the system and results in more accurate simulation results. The method of index reduction mentioned earlier is quite complicated and rigorous and requires additional equations and variables; for this reason, Baumgarte [11] suggests a stabilization law for different types of constraints. In this method, the added multipliers μ used in index reduction become obsolete, and the method simplifies differential equations of constrained dynamic systems greatly. The DAE systems obtained from this method have proven to be stable and robust to disturbances, numerical or otherwise.

A system of n particles is described by the equations of motion

$$m_i \ddot{x}_i - F_i = 0. \quad (i = 1, 2, \dots, n) \quad (3.1)$$

Assume the system is subject to a constraint linear in \ddot{x}

$$f(x, \dot{x}, \ddot{x}; t) = \sum_{i=1}^n g_i(x, \dot{x}; t) \ddot{x} + G(x, \dot{x}; t) = 0. \quad (3.2)$$

The equations of motion thus become

$$m_i \ddot{x}_i - F_i = \lambda_i g_i(x, \dot{x}; t), \quad (i = 1, 2, \dots, n) \quad (3.3)$$

where λ_i are the Lagrange multipliers. Solving for \ddot{x} in (3.3) and plugging into (3.2)

$$\lambda = -\frac{\sum \frac{g_i F_i}{m_i} + G}{\sum \frac{g_i^2}{m_i}}, \quad (3.4)$$

which can be used to solve (3.3) to finally get

$$m_i \ddot{x}_i - F_i = -\frac{\sum \frac{g_k F_k}{m_k} + G}{\sum \frac{g_k^2}{m_k}} g_i. \quad (3.5)$$

Equations (3.1-3.5) show that if a constraint is linear in acceleration, it could be eliminated by solving for the Lagrange multipliers analytically and the system would satisfy the same dynamics.

In the case of holonomic and nonholonomic constraints, holonomic constraints are a set of constraints defined by

$$N_h(x; t) = 0, \quad (3.6)$$

differentiating (3.6) twice results in a constraint linear in \ddot{x}

$$\dot{N}_h = \sum \frac{\partial N_h}{\partial x_i} \dot{x}_i + \frac{\partial N_h}{\partial t} = 0, \quad (3.7)$$

$$\ddot{N}_h = \sum \frac{\partial N_h}{\partial x_i} \ddot{x}_i + G(x, \dot{x}; t) = 0, \quad (3.8)$$

where $g_i = \frac{\partial N_h}{\partial x_i}$ and $f = \dot{N}_h$.

For the case of nonholonomic constraints, the equations are

$$N_{nh}(x, \dot{x}; t) = 0, \quad (3.9)$$

where differentiating once gives

$$\dot{N}_{nh} = \sum \frac{\partial N_{nh}}{\partial \dot{x}_i} \ddot{x}_i + G(x, \dot{x}; t) = 0, \quad (3.10)$$

with $g_i = \frac{\partial N_{nh}}{\partial \dot{x}_i}$ and $f = \dot{N}_{nh}$.

The differential equations obtained from the constraint differentiation (3.8) and (3.10) can be unstable and lead to large inaccuracies for small drift as seen in the previous section. Looking into the equations of the holonomic constraints more thoroughly, and knowing that the system defined in (3.5) ensures $f = \dot{N}_h = 0$, then taking initial conditions on the constraint $N_h(0) = 0, \dot{N}_h(0) = 0$, results in $N_h = 0 \quad \forall t$. The nonholonomic case gives the same results for a similar method. Inaccuracies arise when numerical errors occur in the integration and lead to larger system errors due to the unstable fashion of the constraints. To solve for this problem, Baumgarte suggests stabilizing the constraint f by using

$$f = \ddot{N}_h + 2\alpha \dot{N}_h + \beta^2 N_h = 0, \quad (3.11)$$

in the holonomic case, and

$$f = \dot{N}_{nh} + \gamma N_{nh} = 0, \quad (3.12)$$

in the nonholonomic case. In equations (3.11) and (3.12), α, β , and γ are positive constants, ensuring asymptotic stability for the constraints. For holonomic constrained systems of the form

$$\begin{aligned} \ddot{y} - f(\dot{y}, y, \lambda, t) &= 0, \\ c(y, t) &= 0, \end{aligned} \quad (3.13)$$

this new constraint, assuming it isn't explicitly dependent on time, takes the form

$$f = \frac{\partial^2 c}{\partial y^2} \dot{y}^2 + \frac{\partial c}{\partial y} \ddot{y} + 2\alpha \frac{\partial c}{\partial y} \dot{y} + \beta^2 c = 0. \quad (3.14)$$

Nonholonomic constrained systems take the form

$$\begin{aligned} \ddot{y} - f(\dot{y}, y, \lambda, t) &= 0, \\ c(\dot{y}, t) &= 0, \end{aligned} \quad (3.15)$$

the stabilized form for the constraint is

$$f = \frac{\partial c}{\partial y} \dot{y} + \gamma c = 0. \quad (3.16)$$

Comparing these equations with those obtained from the index reduction method above, this stabilization method gives easier systems to solve. After obtaining the stable constraint equation, one can solve for the Lagrange multipliers λ and plug them into the equations of motion, to obtain implicit ODEs. One issue with this method is the choice of α, β and γ as they are decay factors, and need to be chosen based on the requirements of the system.

In regards to unifying holonomic and nonholonomic constraints, Yun and Sarkar [22] are motivated by Baumgarte's stable constraint formulation to produce velocity level constraints from both holonomic and nonholonomic constraints. By applying equation (3.12) on holonomic constraints, they obtain stable constraints linear in \dot{x} which they then add into the equations of motion to obtain a robust constrained system. The general Euler-Lagrange equations reached are the same obtained in (2.21), but with the holonomic constraint $C(q)$ taken instead to be $\dot{C}(q) + \sigma C(q) = 0$, similar to (3.12). An analysis of this equation by Yun shows its stability, as solving for $C(q)$ results in

$$C(q) = C_0 \exp -\sigma t, \quad (3.17)$$

which converges to C_0 for $\sigma > 0$. The method demonstrated by Yun, though, is not as stable as that of Baumgarte, nor is it reduced in terms of its index.

Pendulum Constraint based on Baumgarte The constraint equation of the pendulum and its derivatives seen in (2.52) can be plugged into Baumgarte's stabilization equation to give

$$\frac{2y(-gm + \tau_y + 2\lambda y)}{m} + \beta^2(-l^2 + x^2 + y^2) + \frac{2x(\tau_x + 2\lambda x)}{m} + 2u^2 + 4\alpha(ux + vy) + 2v^2 = 0, \quad (3.18)$$

which give a solution for λ

$$\lambda = \frac{1}{4} \left(\frac{-2y(-gm + 2\alpha mv + \tau_y) + \beta^2 l^2 m - 2m(u^2 + 2\alpha ux + v^2) - 2\tau_x x}{x^2 + y^2} - \beta^2 m \right), \quad (3.19)$$

allowing the replacement in the original equations of motion

$$\begin{aligned} \dot{x} &= u, \\ \dot{y} &= v, \\ m\ddot{u} &= \frac{1}{2}x \left(\frac{-2y(-gm + 2\alpha mv + \tau_y) + \beta^2 l^2 m - 2m(u^2 + 2\alpha ux + v^2) - 2x\tau_x}{x^2 + y^2} - \beta^2 m \right) + \tau_x, \\ m(g + \ddot{v}) &= \frac{1}{2}y \left(\frac{-2y(-gm + 2\alpha mv + \tau_y) + \beta^2 l^2 m - 2m(u^2 + 2\alpha ux + v^2) - 2x\tau_x}{x^2 + y^2} - \beta^2 m \right) + \tau_y. \end{aligned} \quad (3.20)$$

Nonholonomic Constraint Stabilization For the case of the nonholonomic disk in the plane, the constraints seen in equation (2.26), repeated here

$$\begin{aligned} \dot{x} - r \sin(\theta) \dot{\phi} &= 0, \\ \dot{y} - r \cos(\theta) \dot{\phi} &= 0, \end{aligned} \quad (3.21)$$

the constraints are stabilized using equation (3.12) to give

$$\begin{aligned} \frac{r^2 \cos^2(\theta) (\lambda_2 \tan(\theta) + \lambda_1)}{J_2} + \frac{\lambda_1}{m} + r \dot{\theta} \sin(\theta) \dot{\phi} + \gamma (\dot{x} - r \cos(\theta) \dot{\phi}) &= 0, \\ \frac{J_2 \lambda_2 + m (r (r \sin(\theta) (\lambda_2 \sin(\theta) + \lambda_1 \cos(\theta))) - J_2 \dot{\phi} (\gamma \sin(\theta) + \dot{\theta} \cos(\theta))) + \gamma J_2 \dot{y}}{J_2 m} &= 0, \end{aligned} \quad (3.22)$$

where solving for λ_1 and λ_2 gives

$$\begin{aligned} \lambda_1 &= \frac{\gamma m^2 r^2 u \cos(2\theta)}{2(J_2 + mr^2)} - \frac{\gamma m^2 r^2 u}{2(J_2 + mr^2)} + \frac{\gamma m^2 r^2 v \sin(2\theta)}{2(J_2 + mr^2)} - \frac{m^2 r^3 \omega_1 \omega_2 \sin(\theta)}{J_2 + mr^2} \\ &\quad + \frac{\gamma J_2 m r \omega_2 \cos(\theta)}{J_2 + mr^2} - \frac{J_2 m r \omega_1 \omega_2 \sin(\theta)}{J_2 + mr^2} - \frac{\gamma J_2 m u}{J_2 + mr^2}, \\ \lambda_2 &= \frac{\gamma m^2 r^2 u \sin(2\theta)}{2(J_2 + mr^2)} - \frac{\gamma m^2 r^2 v \cos^2(\theta)}{J_2 + mr^2} + \frac{m^2 r^3 \omega_1 \omega_2 \cos(\theta)}{J_2 + mr^2} \\ &\quad + \frac{\gamma J_2 m r \omega_2 \sin(\theta)}{J_2 + mr^2} + \frac{J_2 m r \omega_1 \omega_2 \cos(\theta)}{J_2 + mr^2} - \frac{\gamma J_2 m v}{J_2 + mr^2}. \end{aligned} \quad (3.23)$$

Finally plugging λ_1 and λ_2 back into the equations of motion gives a system of implicit ODEs.

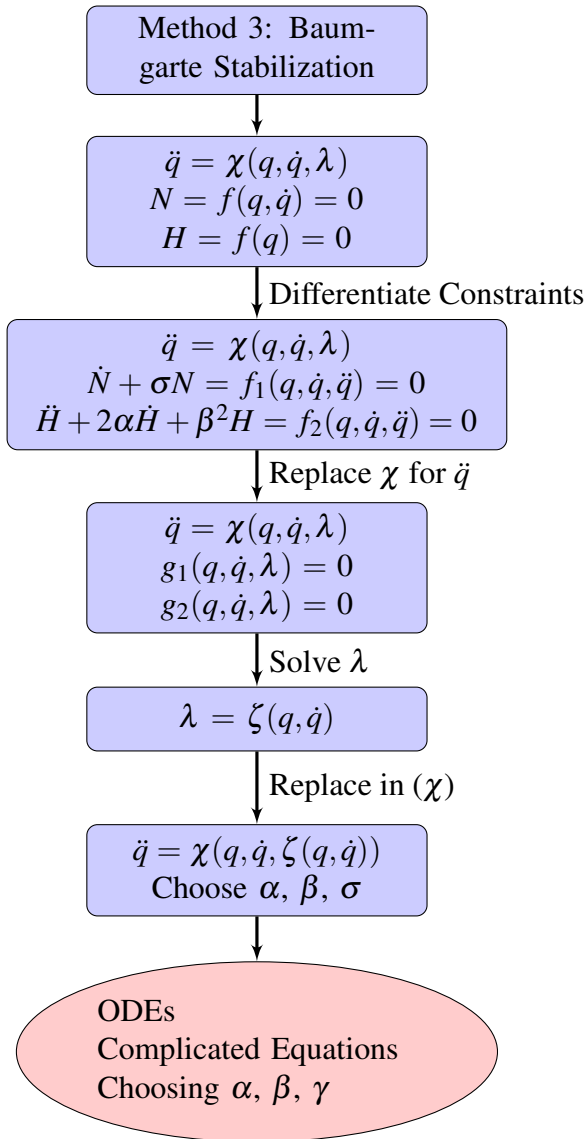


Figure 3.1: Third method to simplify constrained mechanical systems

3.1.1 Simulation-Friendly Method to Simplify DAEs

In section 2.2, it was shown that the high index of a system makes it difficult to solve differential algebraic equations that result for the Lagrangian formulation. An index reduction method was introduced where some essential notions on differential algebraic equations were presented. One of the notions of DAEs that were useful in studying dynamic systems is that of the minimum index equivalent. The equations of motion of a mechanical system have a high index solely due to the Lagrange multipliers because the mass matrix, as established earlier, is always non-singular, and the accelerations can be solved for. The minimum index equivalent can be applied to systems which have purely algebraic variables, such as mechanical systems with λ s. Introducing $\dot{\lambda}$ instead of just λ into constrained mechanical systems reduces their index by 1, so purely nonholonomic systems are reduced to index 1, while holonomic systems are reduced to index 2. For nonholonomic systems of the form

$$\begin{aligned} M(q)\ddot{q} + C(q, \dot{q})\dot{q} + g(q) + b(q)\dot{q} &= \tau + A(q)^T \lambda, \\ N(q, \dot{q}) &= 0, \end{aligned} \quad (3.24)$$

this greatly helps in simulation, as reducing the index of the system to 1 allows the use of available solvers without requiring any additional index reduction techniques. For holonomic systems or mixed systems of the form

$$\begin{aligned} M(q)\ddot{q} + C(q, \dot{q})\dot{q} + g(q) + b(q)\dot{q} &= \tau + A_1(q)^T \lambda_1 + A_2(q)^T \lambda_2, \\ N(q, \dot{q}) &= 0, \\ H(q) &= 0, \end{aligned} \quad (3.25)$$

this reduces the index to 2, thus requiring less work to reduce the index further.

In section 3.1, Baumgarte suggested a method that solves for the whole set of Lagrange multipliers and replaces in the original equations of motion to obtain implicit ODEs, *i.e.* index 0. The obtained equations can sometimes be problematic to deal with, as the system can get more and more complicated, the equations also get more and more complicated. Solving for the generalized acceleration followed by solving for λ s and replacing can be time demanding and does not guarantee an easier time in simulation. An alternative is also to use the minimum index equivalent of the system, and instead of solving for λ s, leaving the stabilized constrained equations as part of the set, where the new set with $\dot{\lambda}$ instead of λ results in simpler ODEs. In this case, general systems of the form (3.25) result in

$$\begin{aligned} M(q)\ddot{q} + C(q, \dot{q})\dot{q} + g(q) + b(q)\dot{q} &= \tau + A(q)^T \dot{\lambda}, \\ \dot{N}(q, \dot{q}) + \gamma N(q, \dot{q}) &= 0, \\ \ddot{H}(q) + 2\alpha\dot{H}(q) + \beta^2 H(q) &= 0, \end{aligned} \quad (3.26)$$

where solving for \ddot{q} and replacing in the bottom equations results in ordinary differential equations.

Two drawbacks to this method are the initialization of the system as we have increased its order requiring more initial conditions, and the choice of α , β , and γ .

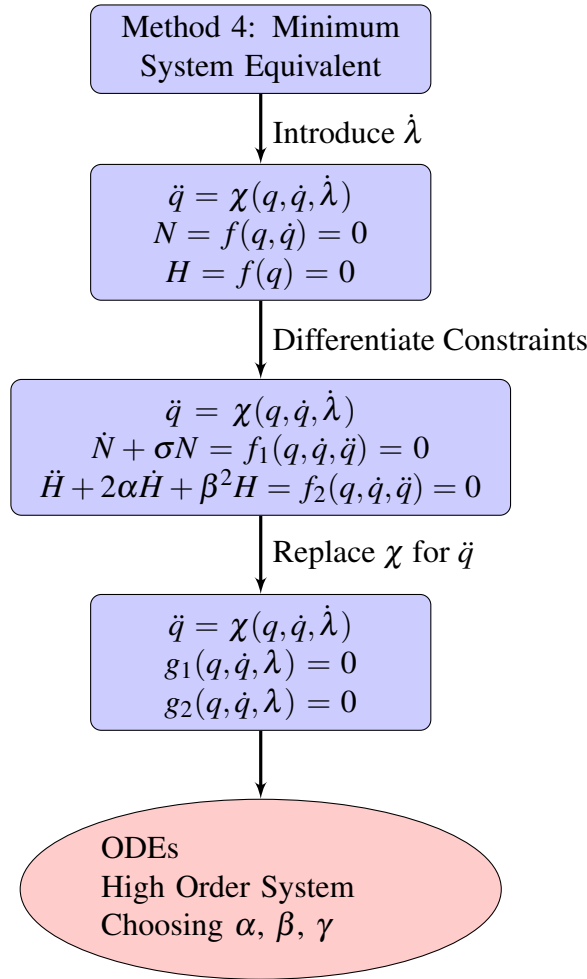


Figure 3.2: Fourth method to simplify constrained mechanical systems

3.2 Linearization and Control

This section looks to study the application of linear control on nonlinear dynamic systems acquired from the Lagrangian formulation and the stabilization method introduced earlier. The linearization process is first introduced, followed by a study of controllability. The Riccati equation is then introduced in order to find the controller gains for robust trajectory tracking.

3.2.1 Linearization

Consider a nonlinear system

$$\begin{aligned} \dot{x}(t) &= f(x(t), u(t)), \\ y(t) &= g(x(t), u(t)), \end{aligned} \tag{3.27}$$

with state vector x , input vector u , and output vector y . It is often useful to define a linear equivalent to systems of the form (3.27) to allow for the implementation of simpler analysis and linear control techniques. This process, termed linearization, provides a linear approximation of the system within a certain neighborhood of an equilibrium point (\bar{x}, \bar{u}) or an equilibrium trajectory $(\bar{x}(t), \bar{u}(t))$.

Consider the more general case of the equilibrium trajectory $(\bar{x}(t), \bar{u}(t))$. A Taylor series expansion of f and g result in the approximation

$$\begin{aligned} f(x(t), u(t)) &\approx f(\bar{x}(t), \bar{u}(t)) + A(x(t) - \bar{x}(t)) + B(u(t) - \bar{u}(t)), \\ g(x(t), u(t)) &\approx g(\bar{x}(t), \bar{u}(t)) + C(x(t) - \bar{x}(t)) + D(u(t) - \bar{u}(t)), \end{aligned} \quad (3.28)$$

where

$$A(t) = \left. \frac{\partial f}{\partial x} \right|_{x=\bar{x}, u=\bar{u}}, \quad B(t) = \left. \frac{\partial f}{\partial u} \right|_{x=\bar{x}, u=\bar{u}}, \quad C(t) = \left. \frac{\partial g}{\partial x} \right|_{x=\bar{x}, u=\bar{u}}, \quad D(t) = \left. \frac{\partial g}{\partial u} \right|_{x=\bar{x}, u=\bar{u}}. \quad (3.29)$$

By defining deviations from the equilibrium trajectory

$$\tilde{x}(t) = x(t) - \bar{x}(t), \quad \tilde{u}(t) = u(t) - \bar{u}(t), \quad \tilde{y}(t) = y(t) - g(\bar{x}(t), \bar{u}(t)),$$

and noting that

$$\dot{\tilde{x}}(t) = f(\bar{x}(t), \bar{u}(t)), \quad (3.30)$$

the linearized system in standard state space form is computed

$$\begin{aligned} \dot{\tilde{x}}(t) &= A(t)\tilde{x}(t) + B(t)\tilde{u}(t), \\ \tilde{y}(t) &= C(t)\tilde{x}(t) + D(t)\tilde{u}(t), \end{aligned} \quad (3.31)$$

where the nonlinear system can be studied under the scope of time-varying linear systems[23].

In the case of nonlinear dynamic systems void of constraints, the second order differential equations derived from the Euler-Lagrange formulation are

$$M(q)\ddot{q} + C(q, \dot{q})\dot{q} + g(q) + b(q)\dot{q} = \tau, \quad (3.32)$$

assuming the mass matrix M is invertible, the generalized accelerations can be computed

$$\ddot{q} = M^{-1}(\tau - C(q, \dot{q})\dot{q} - g(q) - b(q)\dot{q}). \quad (3.33)$$

A set of n new variables and equations to account for the generalized velocities are introduced to reduce the system to a first order set of equations

$$\begin{aligned} p &= \dot{q}, \\ \dot{p} &= M(q)^{-1}(\tau - C(q, p)p - g(q) - b(q)p), \end{aligned} \quad (3.34)$$

where the nonlinear function f is defined as the right hand side of (3.34), the states are $(q, p)^T$ and the output can be defined based on the requirements of the system.

Holonomic and nonholonomic constraints in dynamic systems add a degree of difficulty to the linearization process. This difficulty is a direct result of algebraic Lagrange multipliers that need to be computed alongside the generalized coordinates and velocities of the system. The algebraic nature of the multipliers presents a dilemma when choosing the states of the system, and computing their time derivatives. It is clear that λ s are to be introduced into the state vector, and the stabilization method with differentiated λ s provides the ideal framework for this linearization process.

Using the equations (3.26), one can repeat the previous process to obtain the set of first order equations

$$\begin{aligned} p &= \dot{q}, \\ \dot{p} &= M(q)^{-1}(\tau + A(q)^T \dot{\lambda} - C(q, p)p - g(q) - b(q)p), \\ \dot{N}(q, p) + \gamma N(q, p) &= 0, \\ \ddot{H}(q) + 2\alpha \dot{H}(q) + \beta^2 H(q) &= 0. \end{aligned} \tag{3.35}$$

It is then possible to compute $\dot{\lambda}$ as a function of q and p using the constraint equations to obtain the desired set of nonlinear equations, tailored for linearization.

Defining the set $X = (q, p, \lambda)^T$ as the states of the system and $U = \tau$ as the inputs, the dynamic equations take the form

$$\dot{X} = F(X, U). \tag{3.36}$$

The linearization process provides the required matrices A and B to proceed with controller design.

3.2.2 Controllability and Decomposition of Uncontrollable Systems

Many system models start facing problems when their controller design is tackled and a controller cannot be simply implemented. This is often due to stability and controllability issues in the system. A fully state controllable system is always sought after, but when controllability is lacking, the system can be decomposed and controlled based on its controllable subsystem.

The controllability of a system of the form $\dot{X} = AX + BU$ is studied using the controllability matrix of the system defined by the state and input matrices A and B as

$$\mathcal{C} = [B, AB, \dots, A^{n-1}B], \tag{3.37}$$

where A is $n \times n$ and B is $n \times m$. The system is fully state controllable if $\dim(\mathcal{C}) = n$, but this is often not the case and a subsystem can be defined based on the controllable states.

To define this subsystem, a transformation P is defined

$$P = [X \quad Y], \tag{3.38}$$

where X is an $n \times c$ matrix whose columns are linearly independent columns of \mathcal{C} and c is the dimension of \mathcal{C} . Y is an $n \times (n - c)$ matrix chosen so that P is nonsingular [24]. P^{-1} can then be partitioned as

$$P^{-1} = \begin{bmatrix} M \\ N \end{bmatrix}, \quad (3.39)$$

where M is $c \times n$ and N is $(n - c) \times n$, giving the transformed A and B matrices

$$\begin{aligned} \bar{A} &= P^{-1}AP = \begin{bmatrix} M \\ N \end{bmatrix} A \begin{bmatrix} X & Y \end{bmatrix} = \begin{bmatrix} MAX & MAY \\ NAX & NAY \end{bmatrix}, \\ \bar{B} &= P^{-1}A = \begin{bmatrix} M \\ N \end{bmatrix} B \begin{bmatrix} X & Y \end{bmatrix} = \begin{bmatrix} MB \\ NB \end{bmatrix}. \end{aligned} \quad (3.40)$$

Finally the controllable subsystem is defined by the top left section of \bar{A} to be $\tilde{A} = MAX$ and the top section of \bar{B} to be $\tilde{B} = MB$, giving the new system

$$\dot{z} = \tilde{A}z + \tilde{B}u. \quad (3.41)$$

A controller is then designed based on (3.41) to give the vector of c gains \tilde{K} . These gains are appended by $(n - c)$ zeros and transformed to represent gains in the original system by

$$K = \tilde{K}P^{-1}. \quad (3.42)$$

Finally, the input is given by

$$U = -KX \quad (3.43)$$

3.2.3 The Linear Quadratic Regulator

After achieving a fully controllable system of the form

$$\dot{x} = Ax + Bu, \quad (3.44)$$

a quadratic regulator cost function [25] for state tracking can be defined as

$$J(x, t) = \int_t^\infty (x^T Qx + u^T Ru) dt, \quad (3.45)$$

where $Q = Q^T > 0$ and $R = R^T > 0$. Matrices Q and R are generally taken to be diagonal matrices where the diagonal elements are considered as weights on tracking the states and inputs.

It can be shown that the optimal cost function is given by

$$J^* = x^T Sx, \quad (3.46)$$

where $S = S^T > 0$. The solution for the matrix S is given by the Riccati equation

$$-\dot{S} = Q - SBR^{-1}B^T S + SA + A^T S, \quad (3.47)$$

with a positive definite boundary condition for S .

Finally the control gains are computed using

$$K = R^{-1}B^T S, \quad (3.48)$$

and the optimal feedback is

$$u^* = -Kx. \quad (3.49)$$

Differential Drive Constrained System Consider a differential drive robot with generalized coordinates

$$q = (x_1, y_1, x_2, y_2, \theta, \phi_1, \phi_2), \quad (3.50)$$

where (x_1, y_1, x_2, y_2) are the coordinates of the two contact points, θ is the orientation in the $x - y$ plane, and (ϕ_1, ϕ_2) are the rotation of each wheel. The choice of coordinates of the contact points is in order to introduce holonomic constraints into the system and study their effect along with nonholonomic constraints on the linearization and control process.

The energy in this system is solely kinetic

$$KE = \frac{1}{2} (\dot{x}_1^2 + \dot{x}_2^2 + \dot{y}_1^2 + \dot{y}_2^2) + \frac{4}{12} \dot{\theta}^2 + \frac{1}{4} \dot{\phi}_1^2 + \frac{1}{4} \dot{\phi}_2^2, \quad (3.51)$$

where the radii, axis length, and total mass are all taken equal to 1.

The system satisfies 3 nonholonomic constraints

$$\begin{aligned} NC_1 &= \frac{1}{2} (\dot{x}_1 + \dot{x}_2) \sin(\theta) + \frac{1}{2} (\dot{y}_1 + \dot{y}_2) \cos(\theta) = 0, \\ NC_2 &= \dot{x}_1 \cos(\theta) + \dot{y}_1 \sin(\theta) - \dot{\phi}_1 = 0, \\ NC_3 &= \dot{x}_2 \cos(\theta) + \dot{y}_2 \sin(\theta) - \dot{\phi}_2 = 0, \end{aligned} \quad (3.52)$$

where the first equation enforces the no-skidding constraint in the lateral direction, and the other two enforce the no-slipping constraints in the forward direction for each wheel. Another two holonomic constraints are added to the system to ensure its rigidity

$$\begin{aligned} HC_1 &= x_1 - x_2 - \sin(\theta) = 0, \\ HC_2 &= y_1 - y_2 + \cos(\theta) = 0. \end{aligned} \quad (3.53)$$

After introducing the differentiated Lagrange multipliers and stabilizing the constraints, a set of equations of the form (3.26) can be derived from the Lagrangian formulation. These equations are transformed to first order by introducing an additional set of velocity states $(u_1, v_1, u_2, v_2, \varepsilon, \omega_1, \omega_2)$ corresponding to $(\dot{x}_1, \dot{y}_1, \dot{x}_2, \dot{y}_2, \dot{\theta}, \dot{\phi}_1, \dot{\phi}_2)$. This first order set of equations can now be linearized around an equilibrium trajectory.

The trajectory chosen is a Dubins' path shown in Fig.3.3, where P_1 is the starting point, P_2 and P_3 are the transition points between the arcs and the line, P_4 is the end point of the second arc, and P_5 is the end point of the trajectory.

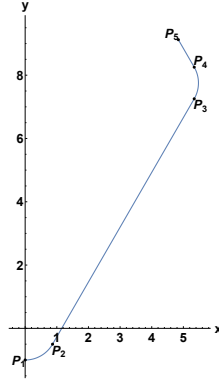


Figure 3.3: Desired equilibrium trajectory

Given the coordinates (x, y) of this trajectory, the equilibrium states can be computed using the equations of the system. The orientation is computed as the inverse tangent of $\frac{y}{x}$

$$\theta = \arctan\left(\frac{y}{x}\right). \quad (3.54)$$

The coordinates of the contact points are computed using the two holonomic constraints (3.53) and the fact that the coordinates of the path is the average of the coordinates of the contact points

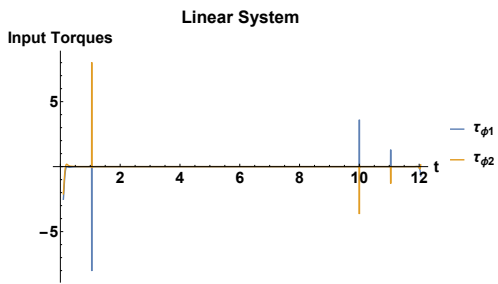
$$\begin{aligned} x_1 - x_2 - \sin(\theta) &= 0, \\ y_1 - y_2 + \cos(\theta) &= 0, \\ \frac{x_1 + x_2}{2} &= x_{traj}, \\ \frac{y_1 + y_2}{2} &= y_{traj}. \end{aligned} \quad (3.55)$$

After that, the rotational velocities of are computed from the no-slipping nonholonomic constraints, NC_2 and NC_3 . The equilibrium inputs and the Lagrange multipliers can be found using the Euler-Lagrange equations after substituting all the computed equilibrium states.

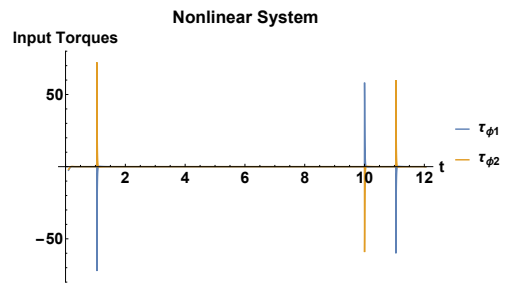
After finding the equilibrium for all the states and inputs, the linearization process can be used to get the matrices A and B of the linearized system from (3.29). The matrices are then used to solve the Riccati equations (3.47) and finally compute the controller gains.

The resulting controller proves to be successful on the linear and nonlinear system, after choosing the proper weights. Noting that the purpose of this controller is trajectory tracking, the weights on the position of the robot are chosen much larger than the rest of the weights, with some emphasis on the orientation and rotational velocities of the wheels.

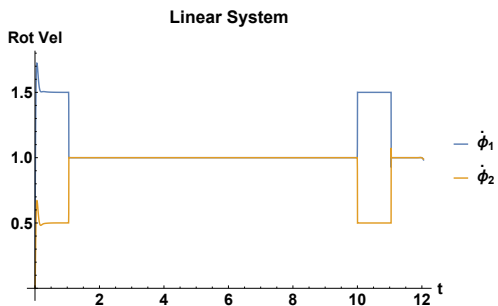
The simulations show how the input torques attempt to achieve the large acceleration required for instantaneous velocity changes, seen for both the linear and nonlinear system in Fig. 3.4a and 3.4b.



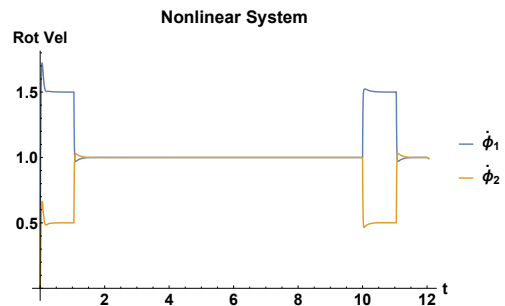
(a) The input torque for the simulated linear system



(b) The input torque for the simulated nonlinear system



(c) Rotational velocity of each wheel for the simulated linear system [3]

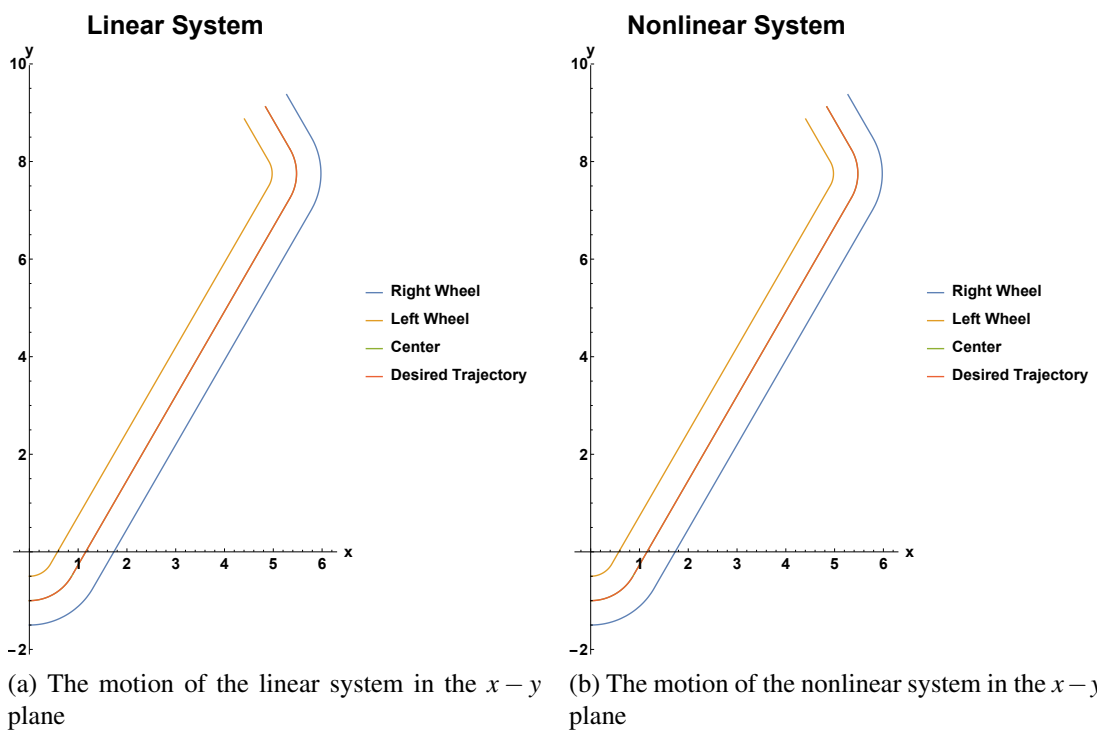


(d) Rotational velocity of each wheel for the simulated nonlinear system

Figure 3.4: The torque inputs and resulting rotational velocities for the simulated linear and nonlinear systems

The rotational velocities required to follow the Dubins' path are seen in Fig. 3.4c and 3.4d, where one wheel rotates faster than another for the circle sections, as compared to equal velocity for the line section.

As a result of this controller, the vehicle is seen following the desired path in both simulations, as seen if Fig. 3.5a and 3.5b.



(a) The motion of the linear system in the $x - y$ plane

(b) The motion of the nonlinear system in the $x - y$ plane

Figure 3.5: Parametric plots of the $x - y$ position of the vehicle simulated using the linear and nonlinear model

Chapter 4

Modeling Flexible Wheels

In this section, the effects of springs and dampers on wheel models will be studied. In addition, the choice of proper stiffness and damping coefficients will be made so that the system requirements are satisfied. The system that will be under study is the rolling disk in two and three dimensions.

4.1 Modeling and Analysis of a Two-Dimensional Flexible Wheel on Flat and Uneven Terrain

In this section, a 2 dimensional model of a wheel moving in the $x - y$ plane over rough terrain will be modeled with a variable diameter instead of a rigid one. The chosen coordinates are (x, θ, r) , where x is the position of the contact point of the wheel, θ is the rolling of the disk, and r is the varying radius. To model this system, 6 points were chosen along the circumference of the wheel that are symmetric with respect to the center point and the system consisting of these points was modeled. The terrain function is termed $f(x)$, giving the wheel-terrain contact angle to be defined as

$$\varepsilon(x) = \arctan(f'(x)). \quad (4.1)$$

The contact point and center point coordinates are defined as

$$P_{contact} = (x, f(x)), \quad (4.2)$$

$$P_{center} = P_{contact} + r \left(\cos(\varepsilon(x) + \frac{\pi}{2}), \sin(\varepsilon(x) + \frac{\pi}{2}) \right). \quad (4.3)$$

The points on the circumference of the disk are defined by

$$P_{i+1} = P_{center} + r \left(\cos(\theta + i\frac{\pi}{3}), -\sin(\theta + i\frac{\pi}{3}) \right), \quad (i = 0, 1, \dots, 5) \quad (4.4)$$

These 6 points hold the mass of the disk equally, such that each has a mass of $\frac{m}{6}$. Springs are present between the center point and all 6 peripheral points, an overall

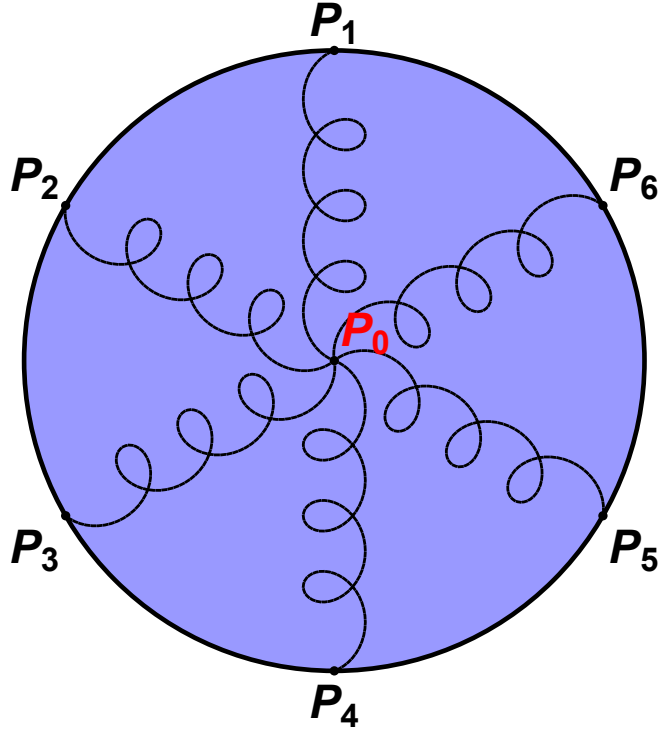


Figure 4.1: The model for the variable diameter disk

stiffness was considered to account for all the springs. The center of mass of the whole system, because of the symmetry as designed, is the center point, with mass m . The energy in the system is thus defined as

$$T = \frac{1}{2} \frac{m}{6} \sum_{i=1}^6 v_i \cdot v_i, \quad (4.5)$$

$$U = \frac{1}{2} k_{tot} (r - r_0)^2 + mgy_{cen}.$$

This system is constrained by a nonholonomic constraint that ensures no slipping in the forward direction. This constraint is written as

$$\dot{x} - r\dot{\theta} \cos(\varepsilon(x)) = 0. \quad (4.6)$$

The constraint is defined using the vector A such that $A^T \dot{q} = 0$, where

$$A = (1, -r \cos(\varepsilon(x)), 0). \quad (4.7)$$

A method for index reduction is used to get the minimum index of the system by introducing the differentiated Lagrange multiplier $\dot{\lambda}$ instead of λ , the constraint forces are

$$f_c = (\dot{\lambda}, -r \cos(\varepsilon(x)) \dot{\lambda}, 0). \quad (4.8)$$

A Rayleigh dissipation function defines the damping in the system as

$$Q = \frac{1}{2}\mu\dot{r}^2. \quad (4.9)$$

The equations of motion of the system, for $f(x) = 0$ are thus defined as

$$m\ddot{x} = \dot{\lambda}, \quad (4.10)$$

$$mr^2\ddot{\theta} + 2mr\dot{r}\dot{\theta} + r\cos(\varepsilon(x))\dot{\lambda} = \tau_\theta, \quad (4.11)$$

$$2m\ddot{r} + mg + kr = mr\dot{\theta}^2 + \mu\dot{r} + kr_0, \quad (4.12)$$

$$\dot{x} - r\dot{\theta}\cos(\varepsilon(x)) = 0. \quad (4.13)$$

This is followed by using the stabilization method for the constraint in the system, so using Baumgarte's method to stabilize the constraints, the new constraint is obtained

$$\dot{\theta}\dot{r} + r(\gamma\dot{\theta} + \dot{\dot{\theta}}) = \gamma\dot{x} + \ddot{x}. \quad (4.14)$$

The final set of equations of motion for the system is

$$m\ddot{x} = \dot{\lambda},$$

$$mr^2\ddot{\theta} + 2mr\dot{r}\dot{\theta} + r\cos(\varepsilon(x))\dot{\lambda} = \tau_\theta, \quad (4.15)$$

$$2m\ddot{r} + mg + kr = mr\dot{\theta}^2 + \mu\dot{r} + kr_0,$$

$$\dot{\theta}\dot{r} + r(\gamma\dot{\theta} + \dot{\dot{\theta}}) = \gamma\dot{x} + \ddot{x}.$$

The parameters used for the system are $m = 1$, $l_0 = 1$, $k_{tot} = 100$, $g = 9.81$, $\mu = -10$, and $\gamma = 1$, where the stiffness and damping coefficients are chosen such that the radius at the chosen constant rotational velocity is less than 10% from the natural spring length, and so that the value reaches this point smoothly and without significant overshoot. The controller used is a PID controller defined as

$$\tau_\theta = \ddot{\theta}_d + k_p(\theta_d - \theta) + k_d(\dot{\theta}_d - \dot{\theta}), \quad (4.16)$$

where the controller gains are $k_p = 100$ and $k_d = 10$.

The effect of the variable radius on the disk moving over flat terrain is first studied, specifically looking at how the radius will change with acceleration. Taking the desired position values to be

$$\theta_{desired} = 0.5t, \quad (4.17)$$

The controller, as seen in Fig. 4.2a, is effective as the rotational velocity reaches the desired value in 0.2s with no overshoot. The radius of the disk also increases, as expected (Fig. 4.2b), based on the acceleration of the disk. This effect provides insight into simulating a vehicle with flexible wheels. Some care should be taken when the results depend highly on the velocity of the system under study, in addition to choosing proper damping and stiffness coefficients.

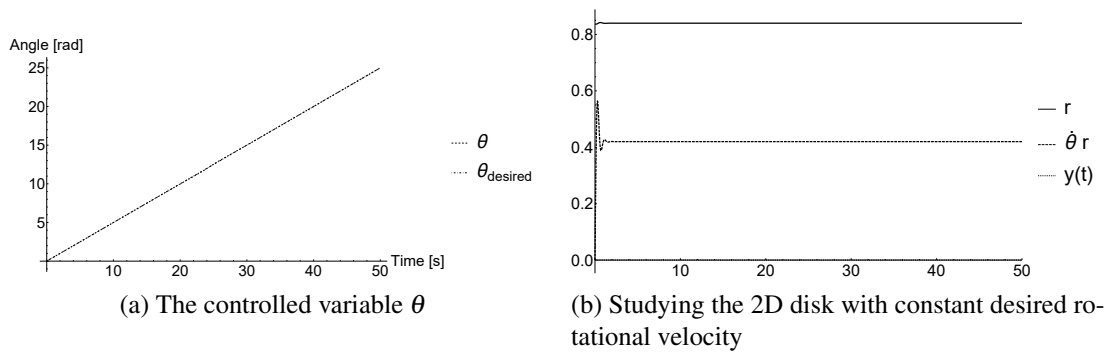


Figure 4.2: Studying the 2D disk over flat terrain for constant velocity

More importantly simulations were performed to study the effect of uneven terrain on the varying radius. The first studies the effect of a single smooth bump defined by

$$f(x) = \exp\left(-\frac{(x-10)^2}{2}\right), \quad (4.18)$$

seen in Fig. 4.3. The control used is the same as before giving the same effect.

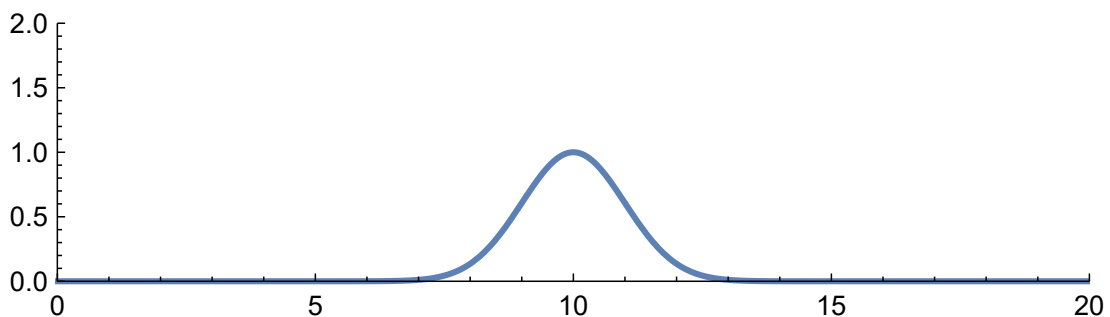


Figure 4.3: Single smooth bump used in 2D simulations

The resulting plot Fig. 4.4 shows the radius increasing on the slopes of the bump. The radius increases as the disk starts climbing the bump to reach a maximum at the inflection point then decrease again as it reaches the top. The process is repeated on the way back down, until it hits flat ground and goes back to its stable value.

Due to this radius change, a velocity change is observed, where the total velocity of the disk is plotted, namely $V = \dot{\theta}r$, versus time. As the disk goes over the bump, an additional velocity term attributed to velocity in the y direction is found. The total velocity of the disk increases over the bump, which may provide some insight for 2-wheeled vehicles traversing rough terrain.

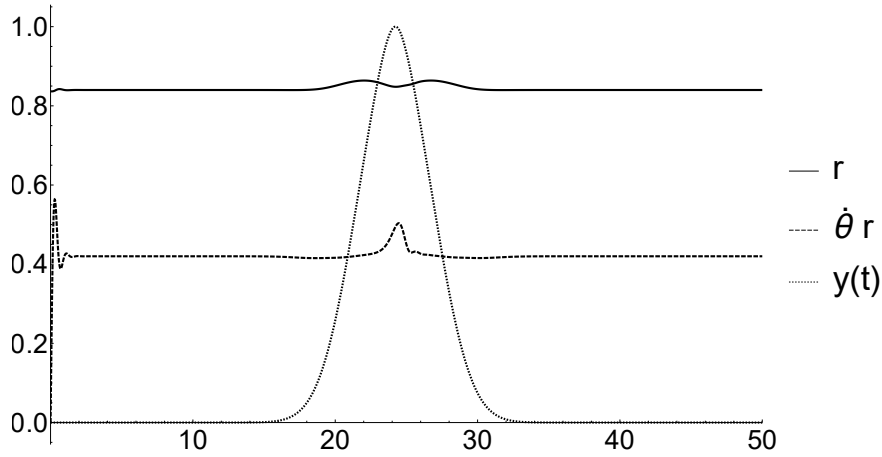


Figure 4.4: Studying the 2D disk over a bump, plotting the radius

4.2 Modeling a Three-Dimensional Wheel over Rough Terrain

Modeling the vehicle over rough terrain has proven to be a much more difficult task than over flat terrain. The main changes when transitioning from flat to rough ground are the fact that the vehicle will no longer be on the same level vertically, and the velocity vectors will be inclined based on the wheel-ground contact angles. To be able to study the full vehicle model, a simpler approach is taken at first, modeling a variable radius disk in 3D going over bumps and studying the simulations.

Any 3D body requires 6 coordinates to be modeled, namely the three spatial coordinates (x, y, z) and three rotational coordinates (θ, β, ϕ) seen in Fig.4.5. Considering the problem at hand, it was more convenient to take instead of the z coordinate, the radius r of the wheel. (x, y) coordinates are assigned to the contact point of the disk with the ground, where its z coordinate is defined by a known terrain function $f(x, y)$. For the purposes of the single disk simulation, consider the inclination angle around the forward direction of the disk $\beta = 0$ at all times. We can thus define the full set of generalized coordinates in our system as

$$q = (x, y, \theta, \phi, r). \quad (4.19)$$

Another orientation, which is the wheel-ground contact angle is defined as

$$\varepsilon(x, y, \theta) = \arctan(\nabla f(x, y) \cdot (\cos \theta, \sin \theta)). \quad (4.20)$$

The disk's center point is found using the contact point position and the rotations as

$$P_{contact} = (x, y, f(x, y)), \quad (4.21)$$

$$P_{center} = P_{contact} + R_{\theta, z} \cdot R_{-\varepsilon - \pi/2, y} \cdot (r, 0, 0), \quad (4.22)$$

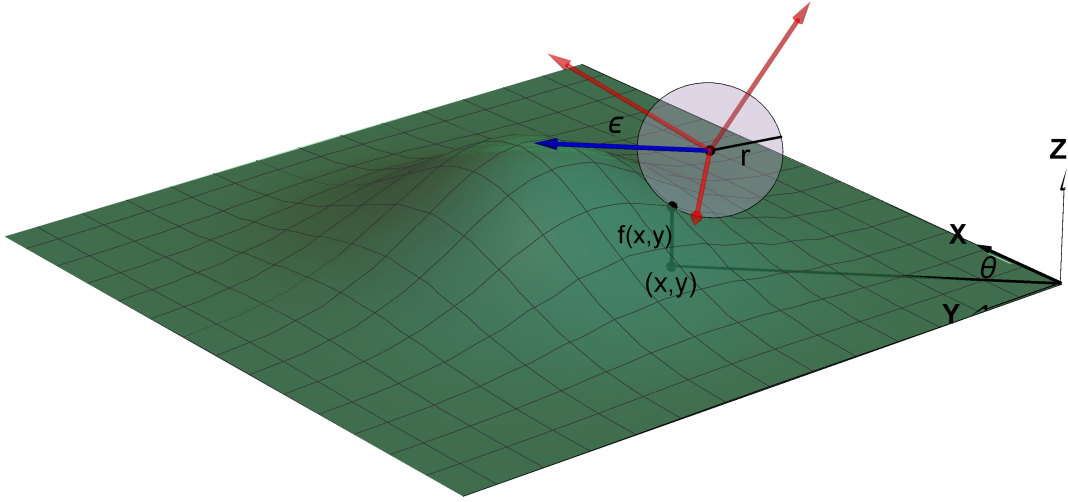


Figure 4.5: 3D disk model and coordinates

where $R_{i,j}$ is a rotation matrix of angle i about axis j . Considering that the center of the disk is the center of mass in the system, the 6 points on the circumference of the disk are defined as

$$P_i = P_{center} + R_{\theta,z} \cdot R_{\phi+\frac{i\pi}{3},y} \cdot (r, 0, 0), \quad (i = 0, 1, \dots, 5) \quad (4.23)$$

the energy and the Lagrangian in the system are

$$T = \frac{1}{2} \frac{m}{6} \sum_{i=1}^6 v_i \cdot v_i, \quad (4.24)$$

$$U = mgz_{center} + \frac{1}{2} k (r - r_i)^2,$$

$$L = T - U.$$

The constraints in the system are the no forward slipping and no lateral skidding constraints on the velocity

$$NHC_1 = \dot{x} - r\dot{\phi} \cos \theta \cos(\epsilon(x, y, \theta)), \quad (4.25)$$

$$NHC_2 = \dot{y} - r\dot{\phi} \sin \theta \cos(\epsilon(x, y, \theta)), \quad (4.26)$$

where the velocity of the contact point was constrained in the x and y directions. In Pfaffian form $A^T \dot{q} = 0$, these constraints give

$$A^T = \begin{pmatrix} 1 & 0 \\ 0 & 1 \\ 0 & 0 \\ -r \cos \theta \cos(\varepsilon(x, y, \theta)) & -r \sin \theta \cos(\varepsilon(x, y, \theta)) \\ 0 & 0 \end{pmatrix}, \quad (4.27)$$

giving the forces

$$f_c = \begin{pmatrix} \lambda_1 \\ \lambda_2 \\ 0 \\ -r\lambda_1 \cos \theta \cos(\varepsilon(x, y, \theta)) - r\lambda_2 \sin \theta \cos(\varepsilon(x, y, \theta)) \\ 0 \end{pmatrix} \quad (4.28)$$

The system is also subject to damping, in addition to the spring stiffness, the Rayleigh dissipation function to describe this effect is

$$D = \frac{1}{2} \mu \dot{r}^2. \quad (4.29)$$

Finally, the equations of motion for the system are

$$\frac{d}{dt} \frac{\partial L}{\partial \dot{q}_i} - \frac{\partial L}{\partial q_i} - \frac{\partial D}{\partial \dot{q}_i} = \tau_i - f_{c,i}, \quad \forall (i = 1, \dots, 5) \quad (4.30)$$

Using Baumgarte stabilization, the constraints are redefined by

$$\frac{dNHC_1}{dt} + \gamma NHC_1 = 0, \quad (4.31)$$

$$\frac{dNHC_2}{dt} + \gamma NHC_2 = 0, \quad (4.32)$$

where γ is a positive constant. The constraints derived using Baumgarte, along with the equations of motion define our full dynamic system.

The disk is first simulated traversing a Gaussian bump, similar to the 2D case, defined by

$$f(x, y) = \exp\left(-\frac{1}{2}(x-10)^2 - \frac{1}{2}y^2\right). \quad (4.33)$$

where the bump is seen in Fig.4.6. The parameters used in the simulations are $m = 1, r_i = 1, k = 100N/m, \mu = -10Ns/m$, and $\gamma = 1$. The initial conditions chosen are such that all variables and their derivatives are 0 except for the radius where $r(0) = r_i - \frac{mg}{k}$.

The results show a slight decrease in x velocity as the disk hits the bump followed by a sharp increase as the disk goes over the bump, then another drop as it hits flat

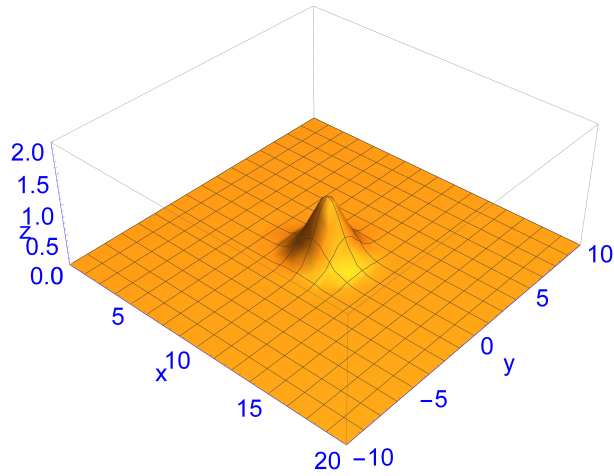


Figure 4.6: Gaussian bump model

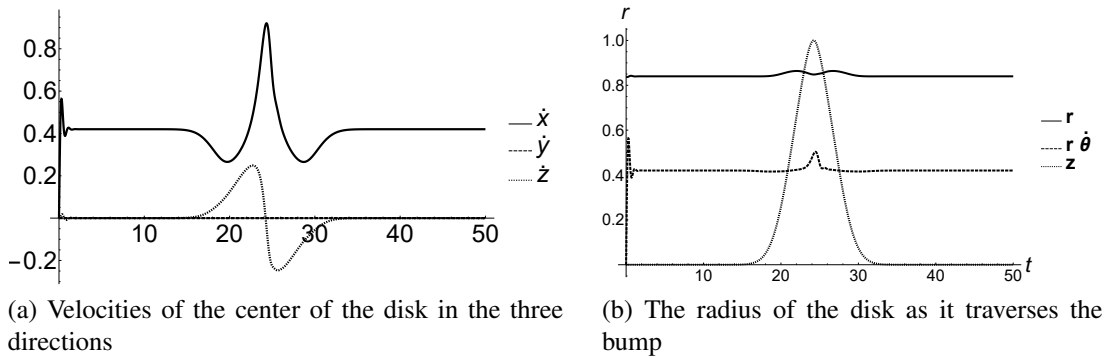


Figure 4.7: Results for the 1st bump model

ground again. The velocity in the z -direction is complementary to the disk going over the bump, seen in Fig. 4.7a.

Looking into these results more thoroughly, the velocity changes are entirely due to the radius changing as the disk goes over the bump with the rotational velocity $\dot{\phi}$ kept constant. The radius of the disk increases as it begins to go up to reach a maximum radius then decreases near the top of the bump, then it increases to the maximum again and starts going back to the constant radius on flat terrain as is seen in Fig. 4.7b. It can be noted that these results are identical to the 2 dimensional case, as the system is effectively the same, only projected to the disk plane.

To study the effect that the bump is having on the velocities, the disk is simulated going over a bump that takes it from 0 height to a constant 0.5 as seen in Fig. 4.8.

The resulting simulation shows a similar effect as before, Fig.4.9a shows that the velocity in x first decreases before increasing to a maximum and then going back to constant as the ground flattens. The velocity in z increases then goes back to 0 soon

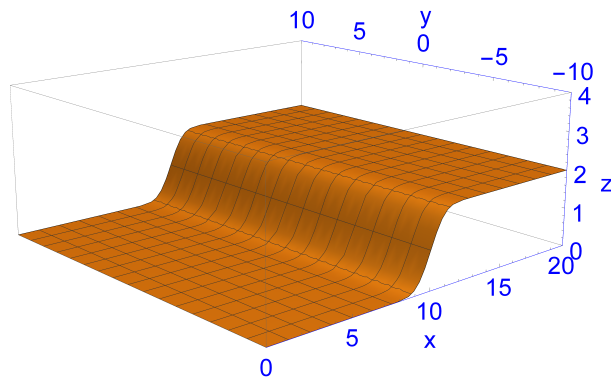


Figure 4.8: 2nd bump model going from 0 to 0.5

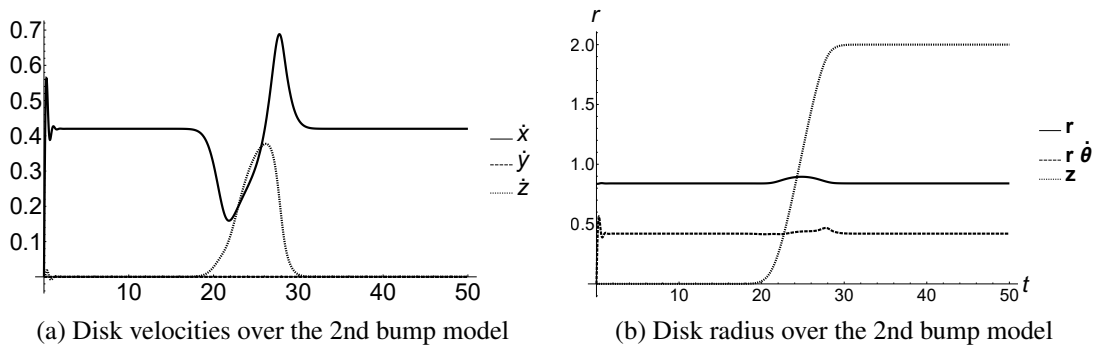


Figure 4.9: Results for 2nd bump model

after. The decrease in x velocity is due to the vehicle's forward direction changing from strictly in the direction of x to being at an angle with the horizontal, thus some of the energy that propelled the disk in the x direction was transferred to the velocity in the z direction. The latter increase is due to the increased radius, thus increased net velocity of the disk. The radius decreases slightly as soon as the disk hits the bump then it increases to reach a maximum before going back to its initial value on flat terrain, as seen in Fig. 4.9b.

4.3 Bump Analysis

To explain the phenomenon of the the radius increasing over the bump, consider the static analysis of a disk on a bump.

In Fig. 4.10, the gravitational pull on the disk is not fully affecting the radius of the disk as it has another component in the direction of motion, in contrast to flat terrain where the direction of motion is orthogonal to the direction of gravity. The resulting

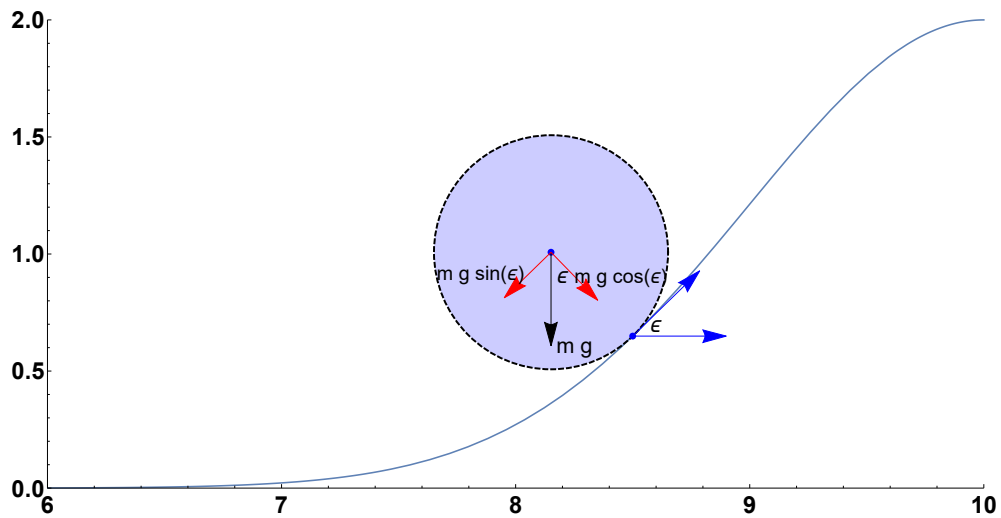


Figure 4.10: A static figure showing the disk on a bump

equations using vectorial analysis are

$$mg \sin \epsilon = ma, \quad (4.34)$$

$$mg \cos \epsilon + k(r - r_0) = 0, \quad (4.35)$$

where the radius is affected by gravity with a coefficient being $\cos \epsilon$ which is only maximal when on flat ground. This results in a slightly lower acceleration due to the added effect of gravity on acceleration, but a slightly larger radius which counteracts the other deficit, resulting in a total increase in acceleration and consequently velocity.

Chapter 5

Modeling, Analysis, and Control

In this chapter, the novel single-actuator design is modeled for mobility over flat and rugged terrain. The model is simulated and analyzed using an open-loop architecture. Based on this analysis, a simpler model is introduced for controller design, where linearization provides the system required for the application of a Linear Quadratic Regulator. The trajectory tracking capabilities of the controlled systems are then studied.

5.1 Initial Vehicle Three-Dimensional Modeling, Analysis, and Simulation over Flat Terrain

The vehicle model, introduced by Sfeir [5], consists of a single actuating disk at the center of a flexible structure. The structure is two variable diameter wheels modeled as spring-dampers, and an axis connecting them, along which the disk moves. The model presented by Sfeir was a simplified 2D model where some of the dynamics were overlooked and simplified. In this section, the full 3D model of this vehicle is studied as it traverses flat and uneven terrain, displaying some path following capabilities.

5.1.1 Vehicle over Flat Terrain

The set of generalized coordinates for the model consists of

$$q = (x, y, \theta, \beta, r, \phi, d, \alpha), \quad (5.1)$$

where (x, y, θ) represent the position and orientation of the vehicle in the $x - y$ plane, β represents the vehicle inclination, which is a direct result of the change in wheel radii, r is a nominal wheel radius, which is the average of the two wheel radii, ϕ is the rolling of the body frame of the vehicle, while d is the distance of the disk from the center of mass of the body along the axis, and finally α is the rotation of the disk.

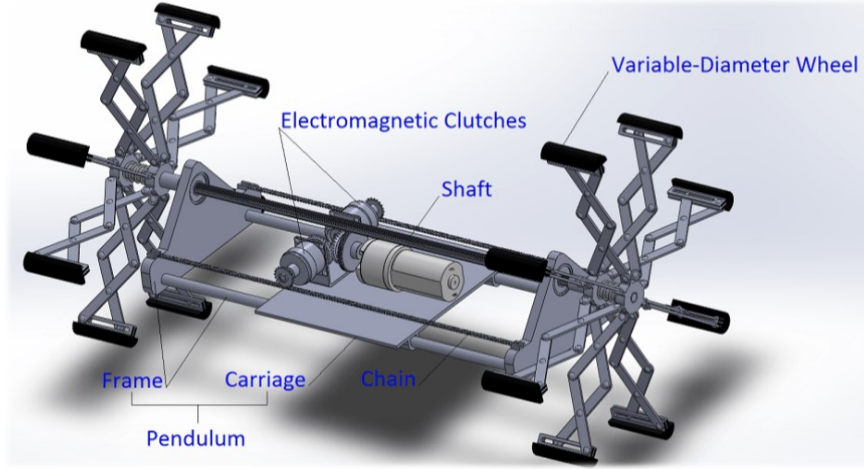


Figure 5.1: Sfeir's Design

β and r were chosen as generalized coordinates instead of the individual wheel radii because this results in a more simplified system, such that β and r are defined as

$$\begin{aligned}\tan \beta &= \frac{r_r - r_l}{2L}, \\ r &= \frac{r_r + r_l}{2},\end{aligned}\quad (5.2)$$

where L is half the axis length.

The centers of mass of the system are separated to be the center of mass of the body and that of the disk. Their coordinates are defined by

$$P_b = \begin{pmatrix} x \\ y \\ r \cos \beta \end{pmatrix}, \quad P_d = \begin{pmatrix} x - d \cos \beta \sin \theta \\ y + d \cos \beta \cos \theta \\ r \cos \beta - d \sin \beta \end{pmatrix}, \quad (5.3)$$

with their velocities being

$$\begin{aligned}V_b &= \begin{pmatrix} \dot{x} \\ \dot{y} \\ \dot{r} \cos(\beta) - \dot{\beta} r \sin(\beta) \end{pmatrix}, \\ V_d &= \begin{pmatrix} -\cos(\beta) \dot{d} \sin(\theta) + d (\dot{\beta} \sin(\beta) \sin(\theta) - \cos(\beta) \dot{\theta} \cos(\theta)) + \dot{x} \\ \cos(\beta) \dot{d} \cos(\theta) - d (\dot{\beta} \sin(\beta) \cos(\theta) + \cos(\beta) \dot{\theta} \sin(\theta)) + \dot{y} \\ \cos(\beta) (\dot{r} - d \dot{\beta}) - \sin(\beta) (\dot{d} + r \dot{\beta}') \end{pmatrix},\end{aligned}\quad (5.4)$$

The energy in the system can thus be found to be

$$KE_b = \frac{1}{2} m_b V_b \cdot V_b + \frac{1}{2} J_{b,1} \dot{\theta}^2 + \frac{1}{2} J_{b,1} \dot{\beta}^2 + \frac{1}{2} J_{b,2} \dot{\phi}^2, \quad (5.5)$$

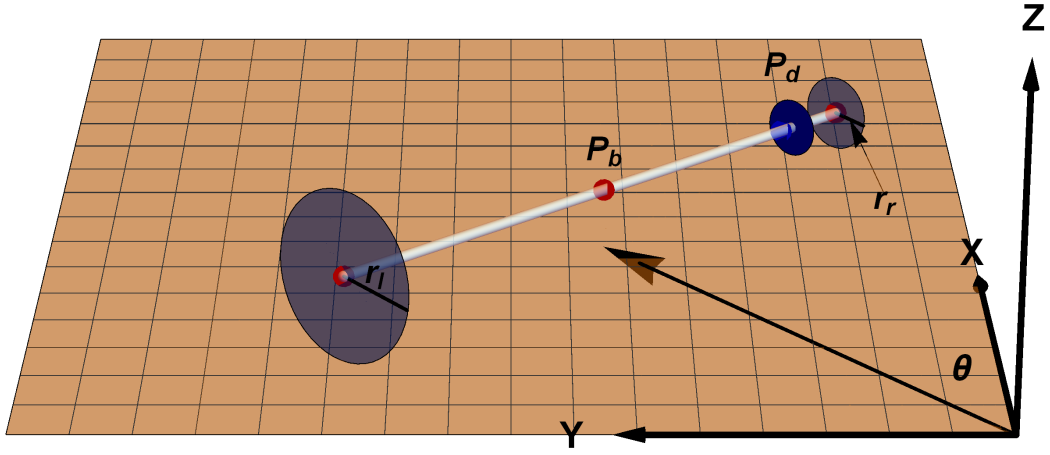


Figure 5.2: The full vehicle model over flat terrain

$$KE_d = \frac{1}{2}m_d V_d \cdot V_d + \frac{1}{2}J_{d,1} \dot{\theta}^2 + \frac{1}{2}J_{d,1} \dot{\beta}^2 + \frac{1}{2}J_{d,2} (\dot{\phi}^2 + \dot{\alpha}^2), \quad (5.6)$$

$$PE = m_b g z_b + m_d g z_d + \frac{1}{2}k(r_r - r_i)^2 + \frac{1}{2}k(r_l - r_i)^2, \quad (5.7)$$

where m_b is the mass of the body, m_d is the mass of the disk, $J_{b,1}$ is the body inertia in θ and β , $J_{b,2}$ is the body inertia in ϕ , $J_{d,1}$ is the disk inertia in θ and β , $J_{d,2}$ is the disk inertia in α and ϕ , r_i is the initial wheel radius, r_r and r_l are the right and left wheel radii, respectively, z_b and z_d are the heights of the vehicle and disk centers of mass, respectively, and k is the spring stiffness.

The constraints on the system are defined as the no forward slipping constraints on each wheel and an averaged no lateral skidding constraint. The equations that describe these 3 constraints are

$$C_1 = V_{w,r} \cdot d_f - r_r \dot{\phi}, \quad (5.8)$$

$$C_2 = V_{w,l} \cdot d_f - r_l \dot{\phi}, \quad (5.9)$$

$$C_3 = \frac{V_{w,r} + V_{w,l}}{2} \cdot d_l, \quad (5.10)$$

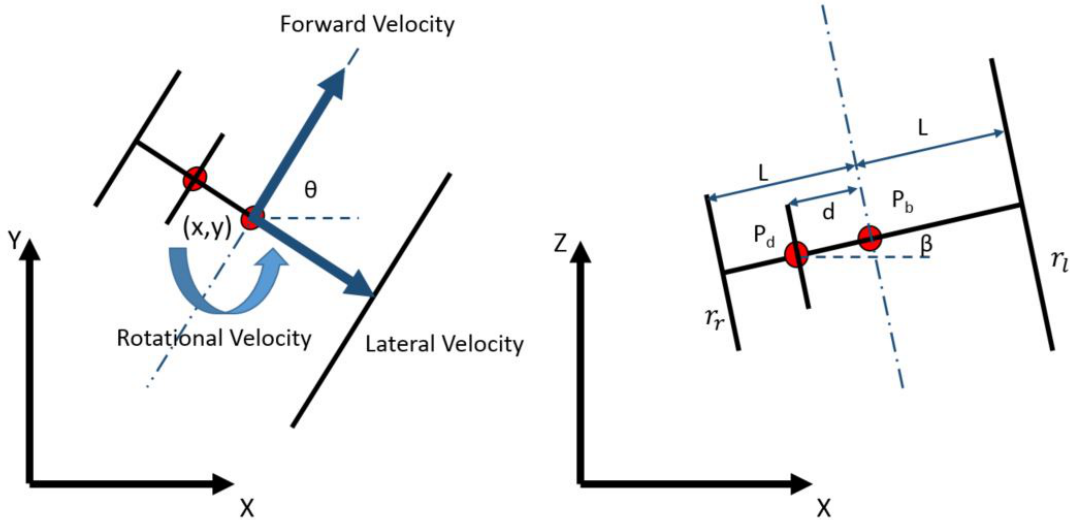


Figure 5.3: Front and top views of the vehicle

where $V_{w,r}$ and $V_{w,l}$ are the velocities of the right and left wheels' center points, respectively, and d_f and d_l are the forward and lateral directions defined as

$$\begin{aligned} d_f &= \begin{pmatrix} \cos \theta \\ \sin \theta \\ 0 \end{pmatrix}, \\ d_l &= \begin{pmatrix} \cos \theta + \frac{\pi}{2} \\ \sin \theta + \frac{\pi}{2} \\ 0 \end{pmatrix}. \end{aligned} \quad (5.11)$$

The constraints are altered to define the motion of the system in a more intuitive way, resulting in the new set

$$C = \begin{pmatrix} \frac{C_1+C_2}{2} \\ C_3 \\ \frac{C_1-C_2}{2L} \cos \beta \end{pmatrix} = \begin{pmatrix} \dot{x} \cos \theta + \dot{y} \sin \theta - r \dot{\phi} \\ -\dot{x} \sin \theta + \dot{y} \cos \theta \\ \dot{\theta} \cos^2 \beta + \dot{\phi} \sin \beta \end{pmatrix}. \quad (5.12)$$

These constraints are defined in their Pfaffian form to get the matrix $A^T \dot{q} = 0$, where

$$A^T = \begin{pmatrix} \cos \theta & -\sin \theta & 0 \\ \sin \theta & \cos \theta & 0 \\ 0 & 0 & -\cos^2 \beta \\ -r & 0 & \sin \beta \\ 0 & 0 & 0 \\ 0 & 0 & 0 \\ 0 & 0 & 0 \\ 0 & 0 & 0 \end{pmatrix}, \quad (5.13)$$

and thus the constraint forces are

$$F_c = A^T \cdot \lambda = \begin{pmatrix} \lambda_1 \cos \theta - \lambda_2 \sin \theta \\ \lambda_1 \sin \theta + \lambda_2 \cos \theta \\ -\lambda_3 \cos^2 \beta \\ -r\lambda_1 + \lambda_3 \sin \beta \\ 0 \\ 0 \\ 0 \\ 0 \end{pmatrix}, \quad (5.14)$$

where $(\lambda_1, \lambda_2, \lambda_3)$ are the set of Lagrange multipliers. The damper is accounted for by using a Rayleigh dissipation function on the right and left wheel radii

$$\begin{aligned} D &= \frac{1}{2} \mu (\dot{r}_r^2 + \dot{r}_l^2) \\ &= \frac{1}{2} \mu \left((\dot{r} - L\dot{\beta} \sec^2 \beta)^2 + (\dot{r} + L\dot{\beta}^2 \sec^2 \beta)^2 \right). \end{aligned} \quad (5.15)$$

Finally, the controlled torques in the system are

$$\tau = \begin{pmatrix} 0 \\ 0 \\ 0 \\ 0 \\ 0 \\ 0 \\ \tau_d \\ \tau_\alpha \end{pmatrix}. \quad (5.16)$$

The final equations of motion for the system are obtained from

$$\frac{d}{dt} \left(\frac{\partial L}{\partial \dot{q}_i} \right) - \frac{\partial L}{\partial q_i} - \frac{\partial D}{\partial \dot{q}_i} = \tau_i - F_{c,i}. \quad (5.17)$$

To simulate the system, the control laws chosen were a PD (proportional and derivative) controlled on α and a proportional controller on d . The torques are defined as

$$\begin{aligned} \tau_\alpha &= \ddot{\alpha}_d + k_{p,\alpha}(\alpha_d - \alpha) + k_{d,\alpha}(\dot{\alpha}_d - \dot{\alpha}), \\ \tau_d &= k_{p,d}(d_d - d), \end{aligned} \quad (5.18)$$

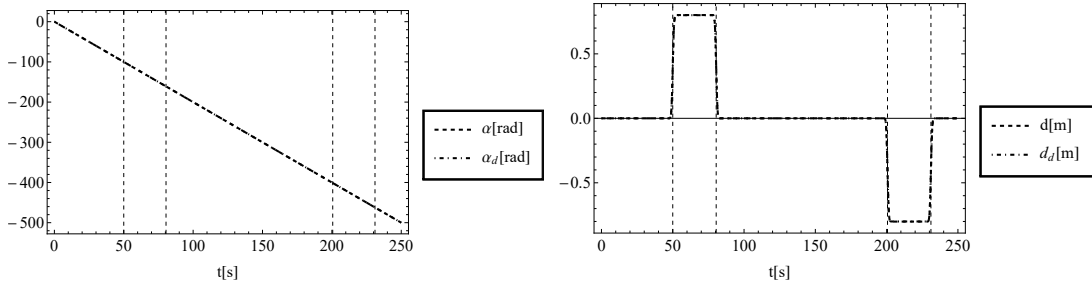
and the system parameters and control gains are seen in table 5.3.

5.1.2 Path Planning over Flat Terrain

To study the model further, the capabilities of this system to follow a Dubins path were looked into, gaining insight into the realistic feasibility of Dubins path. The system

Table 5.1: The proposed system parameter and controller gains.

m_b	1 kg	$k_{p,\alpha}$	5
m_d	16 kg	$k_{d,\alpha}$	1
r_i	0.25 m	$k_{p,d}$	10000
Disk Radius	0.1 m		
k	1000 N/m		
μ	-12 Ns/m		



(a) Controller performance for α , actual versus desired inputs. (b) Controller performance for d , actual versus desired inputs.

Figure 5.4: Controller Performance

was simulated following a Dubins path over $t = 250sec$. The controls are for constant rotational velocity of the wheels, *i.e.* $\dot{\phi} = cst$, and the vehicle follows a Dubins path by oscillating d using the controls as seen in Fig.5.4

The sequence of movements the disk takes according to the controls is

1. Stay in the center of the axis for $t = 50$ seconds
2. Move to the left for $t = T_{c,1}$ seconds
3. Move to the center for $t = T_l$ seconds
4. Move to the right for $t = T_{c,2}$ seconds
5. Move to the center for the remainder of the simulation

The first simulation was done by predicting the vehicle's constant velocity based on the controlled α and choosing the time steps for each turn in the Dubins path accordingly. The resulting choices were $T_{c,1} = T_{c,2} = 30.4607s$ and $T_l = 120.1513s$. The resulting simulations show that our prediction method was lacking as the vehicle's velocity was in fact varying with d , not just α as seen in Fig. 5.5. When d is moved away from the center, in either direction, the rotational velocity of the system $\dot{\phi}$ increased.

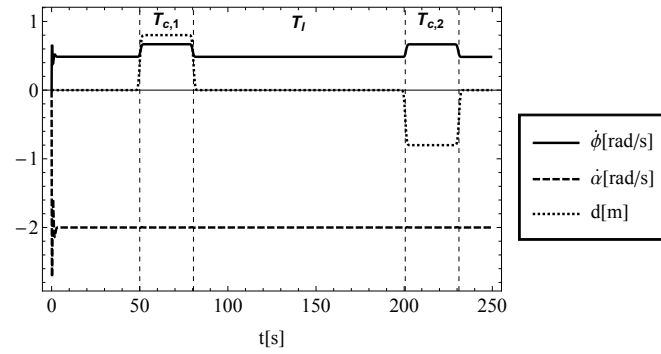


Figure 5.5: Effects of controlled coordinates on driving coordinate $\dot{\phi}$

Fig 5.5 shows that as the vehicle underwent the circle turns along Dubins path, the rotational velocity would increase, effectively disregarding the constant proportionality previously assumed between $\dot{\phi}$ and $\dot{\alpha}$.

Seeing the effect of d on $\dot{\phi}$, some corrections to the control had to be made to follow the path. One way to do this is to vary $\dot{\alpha}$ to counteract the effect of d on the turns of Dubins. A better way which we decided on was to lower the time the vehicle took over the turns accounting for the increased velocity of the vehicle. The new choice of $T_{c,1}$ and $T_{c,2}$ was taken to be $T_{c,1} = T_{c,2} = 22.1323s$. The resulting vehicle velocities, in contrast to constant velocity and the uncorrected simulation are seen in Fig. 5.6.

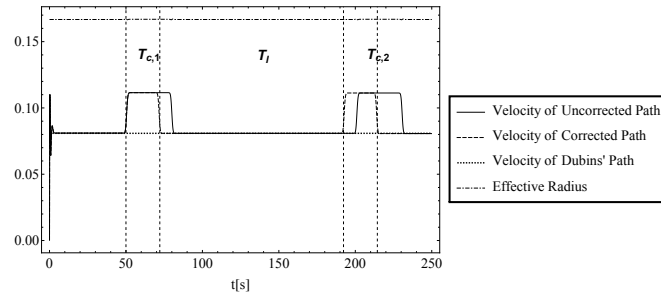


Figure 5.6: The vehicle velocity for the different simulations

Table 5.2: Path errors

Path	Uncorrected Path	Corrected Path
Final pose (x, y, θ)	$(7.86, 13.04, 0.012)$	$(10.06, 9.84, 0.011)$
Position error (m)	3.72	0.168
Orientation error (rad)	0.012	0.011

After correcting for this oversight, the vehicle follows a Dubins path closely but not without some error as seen in Fig.5.7. This is because of the kinematic nature of

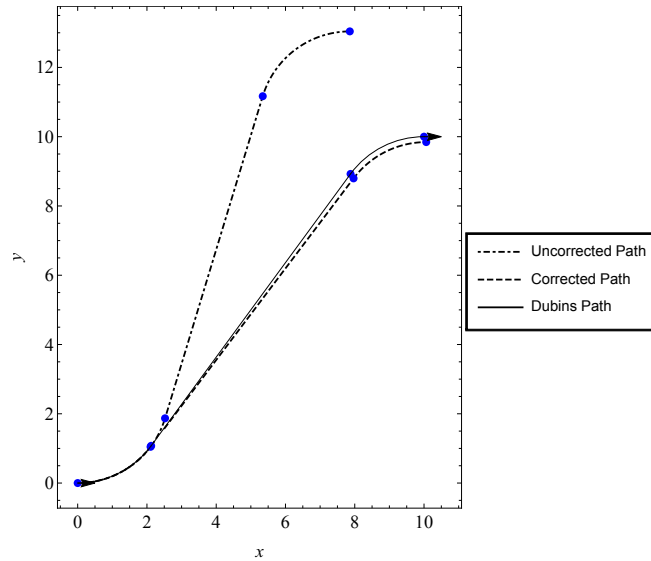


Figure 5.7: Comparison of ideal Dubins path, uncorrected implement path, and corrected implement path.

Dubins model with instantaneous turning rate changes. The system, and any realistic system for that matter, will not be able to follow Dubins exactly. The time correction made a difference of over $3m$ error, making a claim as to how significant the effect of d on the vehicle's velocity is.

5.2 Initial Vehicle Three-Dimensional Modeling, Analysis and Simulation over Rough Terrain

In this chapter, the model for rough terrain simulation is developed, first deriving a model for a single wheel with an added degree of freedom as compared to the model derived in section 4.2, specifically being the inclination angle. The single wheel model is then utilized to develop a full vehicle model. The full model is tested in an attempt to follow a Dubins' path and mitigate the effects of a bump with open loop control.

5.2.1 Single Inclined Wheel over Rough Terrain

A closer inspection of a single wheel over rough terrain, seen in Fig. 5.8, provides a definition for the coordinate frames used to describe the system.

The $x - y - z$ frame is the fixed inertial frame and $u_1 - v_1 - w_1$ is the body frame such that plane P_1 is defined to be the plane of the wheel with the frame origin at the contact point. The frame $u_2 - v_2 - w_2$ is defined from the body frame with a rotation about w_1 by the contact angle. Plane P_2 is defined as the plane normal to \vec{u}_2 passing through the contact point. Using these frames, the full set of coordinates can

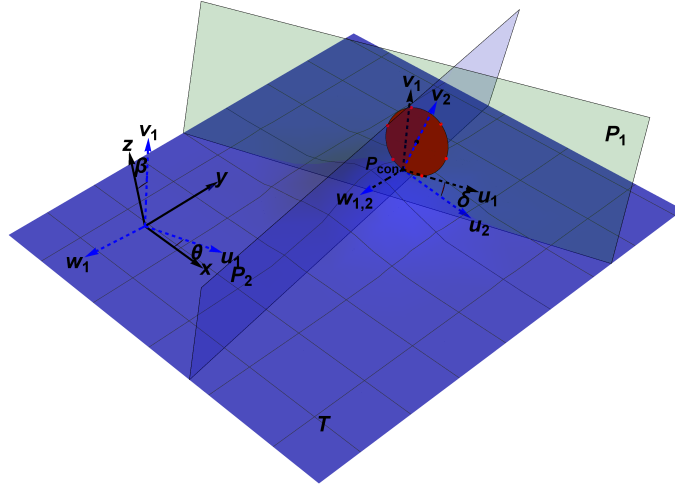


Figure 5.8: Single wheel on rough terrain

be defined. The set of generalized coordinates for a single wheel is

$$q = (x, y, z, r, \theta, \beta, \phi), \quad (5.19)$$

where the coordinates (x, y, z) are those of the contact point in the fixed frame, r is the radius of the wheel, θ is the orientation, defined as the angle between \vec{x} and \vec{u}_1 , β is the inclination, defined as the angle between \vec{z} and \vec{v}_1 .

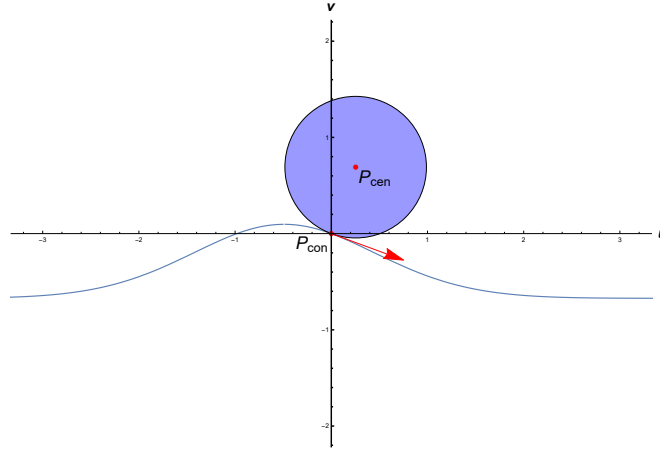


Figure 5.9: Two dimensional projection of terrain surface function onto wheel plane

To simplify the system, the terrain is assumed to be known, *i.e.* z is given as a function of x and y , reducing q to $(x, y, r, \theta, \beta, \phi)$. This information also allows for the definition of the contact angle, δ , as a function of (x, y, θ, β) using the projection of the 3- d surface onto the $u_1 - v_1$ plane, resulting in a 2- d curve with the contact point at the

origin, as seen in Fig. 5.9. The wheel-terrain contact angle can thus be found to be the inverse tangent of the derivative of this intersection at the origin. This wheel-terrain contact angle is essential to define the forward direction along which the wheel moves, as well as the angle of ascent when defining the center of the wheel.

5.2.2 Full System over Rough Terrain

The two wheeled system with the central disk can be generalized from the single wheel system by taking the generalized coordinates

$$q = (x_1, y_1, x_2, y_2, \delta_1, \delta_2, \theta, \beta, \phi, r_1, r_2, d, \alpha), \quad (5.20)$$

where the subscripts 1 and 2 refer to the wheels, and d and α are the actuated motion of the inertial disk. The contact angles δ_i are added to the set of generalized coordinates to ease the computation process during simulations, they are constrained holonomically by equating them to their respective values functions of $(x_i, y_i, \theta, \beta)$. Additionally, lateral contact angles, termed η_i are computed in a similar manner but they were not required in the set of generalized coordinates.

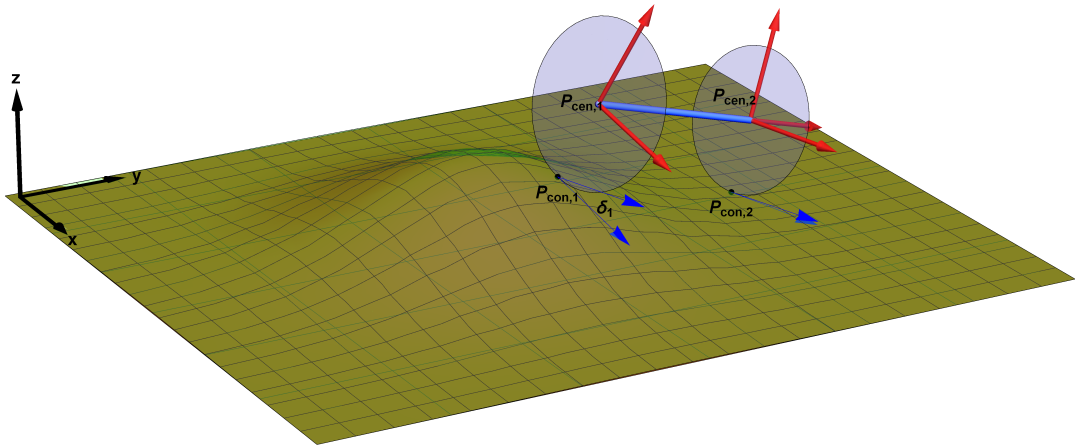


Figure 5.10: Two wheeled system on rough terrain

Given the function $z = f(x, y)$ to define the uneven surface, the positions of the contact points can be defined as

$$P_{con,i} = (x_i, y_i, f(x_i, y_i)). \quad (5.21)$$

The positions of the center points of the wheels are found to be

$$P_{cen,i} = P_{con,i} + R_{\theta,z} \cdot R_{-\beta,x} \cdot R_{-\delta_i,y} \cdot (0, 0, r_i), \quad (5.22)$$

where $R_{a,b}$ is the rotation matrix with an angle a around axis b .

Since the center of mass of the system can be defined using either of the contact points, and the system is modeled as two separate wheels connected by a rigid axis, the rigidity must be enforced through a constraint. The center of the system is used to enforce this constraint. Define, for the time being, the center of the system to be

$$P_{c,1} = P_{cen,1} + R_{\theta,z} \cdot R_{-\beta,x} \cdot (0, \frac{l}{2}, 0), \quad (5.23)$$

where l is the axis length. The center of the disk can be defined as a distance d away from the center of the system along the axis

$$P_d = P_{c,1} - R_{\theta,z} \cdot R_{-\beta,x} \cdot (0, d, 0). \quad (5.24)$$

To account for the diameter changes in the system, a wheel model was developed where an even number of symmetric points are taken along the circumference of the wheel rather than its center. This model captures the dynamics resulting from the diameter variation as well as the rotations and translations in the system. The wheels and disk can thus be described by

$$P_{i,j} = P_{cen,i} + R_{\theta,z} \cdot R_{-\beta,x} \cdot R_{\phi + j\frac{\pi}{3},y} \cdot (r_i, 0, 0), \quad (5.25)$$

$$i = 1, 2, \quad j = 1, 2, \dots, 6,$$

$$P_{d,i} = P_d + R_{\theta,z} \cdot R_{-\beta,x} \cdot R_{\phi + \alpha + j\frac{\pi}{3},y} \cdot (r_d, 0, 0), \quad (5.26)$$

$$i = 1, 2, \dots, 6,$$

where $P_{i,j}$ describes the j th point of the i th wheel, and $P_{d,i}$ describes the i th point of the disk. Taking the time derivatives of equations (5.25) and (5.26) provides all the requirements to define the energy in the system as

$$T = \frac{1}{2} \sum_{i=1}^2 \frac{m_i}{6} \sum_{j=1}^6 V_{i,j} \cdot V_{i,j} + \frac{1}{2} \frac{m_d}{6} \sum_{i=1}^6 V_{d,i}, \quad (5.27)$$

$$U = \sum_{i=1}^2 m_i g z_{cen,i} + m_d g z_d + \frac{1}{2} k \sum_{i=1}^2 (r_i - r_{ini})^2, \quad (5.28)$$

$$L = T - U, \quad (5.29)$$

where m_i and m_d are the respective masses of the wheels and the disk, g is the gravitational acceleration, k is the chosen stiffness, and r_{ini} is the initial radius of the wheels.

System Constraints

For a typical two wheeled vehicle, the constraints are defined as the no-slipping and no-skidding constraints on each wheel. The no slipping constraints are such that the velocity of each contact point in the forward direction is exactly the velocity resulting from the rotation of the wheel

$$N_i = V_{con,i} \cdot R_{\theta,z} \cdot R_{-\beta,x} \cdot R_{-\delta_i,y} \cdot (1, 0, 0) - r_i \dot{\phi} = 0 \quad i = 1, 2. \quad (5.30)$$

For motion on flat terrain, the no-skidding constraints reduce to one because the lateral direction is the same for both wheels, and the constraint is captured with a single equation. For rough terrain motion, Waldron [26] has shown that one or both of the wheels will undergo wheel skid to maintain feasible motion. A friction model is thus introduced into the system where the two skidding constraints are relaxed relative to the motion of the inertial disk. The nonholonomic constraint on the lateral motion of the contact points is defined as

$$\begin{aligned} N_3 = & \frac{1-d}{2} V_{con,1} \cdot R_{\theta,z} \cdot R_{\frac{\pi}{2},x} \cdot R_{\delta_1,z} \cdot R_{-\frac{\pi}{2}} \cdot R_{-\eta_1,z} \cdot (1, 0, 0) \\ & + \frac{1+d}{2} V_{con,2} \cdot R_{\theta,z} \cdot R_{\frac{\pi}{2},x} \cdot R_{\delta_2,z} \cdot R_{-\frac{\pi}{2}} \cdot R_{-\eta_2,z} \cdot (1, 0, 0), \end{aligned} \quad (5.31)$$

where η_i are the lateral angles obtained from the projection. This choice of the multiplying factors accounts for the effect of the mass over the traction in the wheels, where the wheel having a higher mass concentration has more traction and thus less skid.

The system also consists of holonomic constraints, first to account for the rigidity of the system since the model was initialized using two separate wheels. The two possible definitions of the center of the system are utilized. The center of the system, was earlier defined by $P_{c,1}$ and $P_{c,2}$; equating these coordinates results in three holonomic constraints on the system that ensure rigidity

$$H_i = P_{c,1}(i) - P_{c,2}(i) = 0, \quad i = 1, 2, 3. \quad (5.32)$$

The addition of the contact angles δ_i results in two additional holonomic constraints

$$H_{i+3} = \delta_i - g(x_i, y_i, \theta, \beta) = 0, \quad i = 1, 2, \quad (5.33)$$

where $g(x_i, y_i, \theta, \beta)$ is the derived function from the surface projection on the wheel plane.

The obtained constraints are stabilized to give

$$N_{i,s} = \dot{N}_i + \gamma_1 N_i, \quad i = 1, 2, 3, \quad (5.34)$$

$$H_{j,s} = \ddot{H}_j + 2\gamma_2 \dot{H}_j + \gamma_3^2 H_j, \quad j = 1, \dots, 5, \quad (5.35)$$

as in equations (3.12) and (3.11).

The constraint forces in the equations of motion are the same for the stabilized constraints as the normal ones. Using the stabilized constraints, the matrices for the nonholonomic and holonomic constraints are

$$N_{mat}(i, j) = \frac{dN_{i,s}}{d\ddot{q}_j}, \quad H_{mat}(i, j) = \frac{dH_{i,s}}{d\ddot{q}_j}. \quad (5.36)$$

These matrices are joined and multiplied by the set of differentiated Lagrange multipliers

$$F_c = \begin{pmatrix} N_{mat} \\ H_{mat} \end{pmatrix}^T \dot{\lambda}, \quad (5.37)$$

where

$$\dot{\lambda} = (\dot{\lambda}_1 \dot{\lambda}_2 \dot{\lambda}_3 \dot{\lambda}_4 \dot{\lambda}_5 \dot{\lambda}_6 \dot{\lambda}_7 \dot{\lambda}_8)^T \quad (5.38)$$

A Rayleigh dissipation function is used to capture the damping in the wheels

$$D = \frac{1}{2}\mu(\dot{r}_1^2 + \dot{r}_2^2), \quad (5.39)$$

where μ is the damping coefficient.

The generalized forces are those on d and α , giving

$$\tau = (0 \ 0 \ 0 \ 0 \ 0 \ 0 \ 0 \ 0 \ 0 \ 0 \ 0 \ 0 \ \tau_d \ \tau_\alpha). \quad (5.40)$$

Finally the Euler Lagrange equations of motion are

$$\frac{d}{dt} \frac{\partial L}{\partial \dot{q}_i} - \frac{\partial L}{\partial q_i} - \frac{dD}{dq_i} = \tau_i - F_{c,i}, \quad i = 1, \dots, 13, \quad (5.41)$$

which are appended by the stabilized constraint equations

5.2.3 Simulation and Discussion

In this section, the model is verified over flat terrain and the effect of rough terrain is analyzed. An initial simulations studies the system dynamics as it traverses a circle-line-circle Dubins path on flat terrain. This simulation verifies the system dynamics by looking into the forward motion as well as the steering. A second simulation studies the effects of a bump on the system, specifically the trajectory change caused by the rough terrain. This analysis allows for open-loop bump rejection where the system is able to follow the desired path by mitigating the effects of the bump on the steering of the vehicle.

To determine the torques in the system, PD controllers are used to ensure the maintenance of the desired inputs d_d and α_d

$$\tau_d = \ddot{d}_d + k_{d,d}(\dot{d}_d - \dot{d}) + k_{p,d}(d_d - d), \quad (5.42)$$

$$\tau_\alpha = \ddot{\alpha}_d + k_{d,\alpha}(\dot{\alpha}_d - \dot{\alpha}) + k_{p,\alpha}(\alpha_d - \alpha). \quad (5.43)$$

The parameters and controller gains used throughout the simulations are seen in table 5.3.

Table 5.3: The proposed system parameters and controller gains.

m_d	4 kg		
m_1, m_2	0.5 kg	$k_{p,\alpha}$	100
r_i	0.75 m	$k_{d,\alpha}$	10
Disk Radius	0.4 m	$k_{d,d}$	100
k	25 N/m	$k_{p,d}$	10000
μ	-12 Ns/m		
$\gamma_1, \gamma_2, \gamma_3$	12		

Flat Terrain Simulation

The first simulation is given a constant rotational velocity for the disk, and a lateral motion at predetermined time step to account for the steering based on the circular sections of the Dubins path. The disk mass is moved as seen in Fig. 5.11 based on a Dubins path going from (0,0) with zero orientation to (30,30) with with zero orientation. The simulation begins with zero steering as the system reaches a stable velocity, then the disk is moved to one side, back to the center and to the other side to produce a circle-line-circle trajectory.

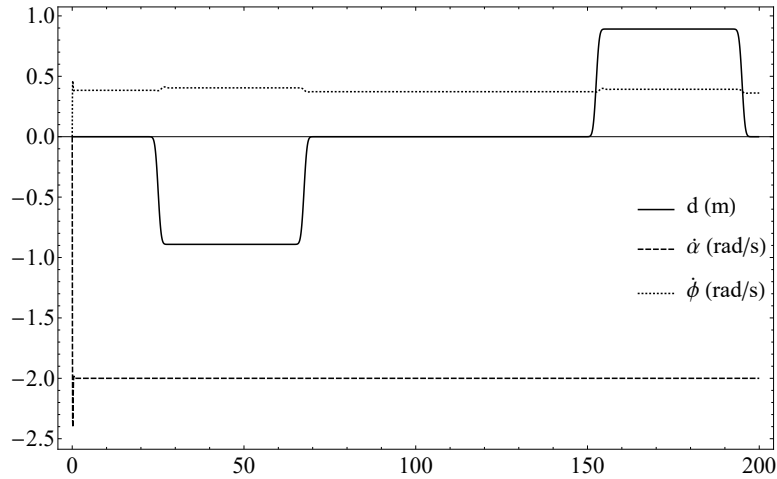


Figure 5.11: The variation of d , $\dot{\alpha}$, and $\dot{\phi}$

The system observed follows the desired path, reaching the final point with high accuracy, as seen in Fig. 5.12.

The final position of the system (29.3948, 29.3167) shows an error due to the dynamics of the system, as compared to the purely kinematic Dubins model. This error is a result of the impossibility to achieve infinite acceleration as the system transitions between the circle and line sections of the trajectory. In addition a slight velocity changes

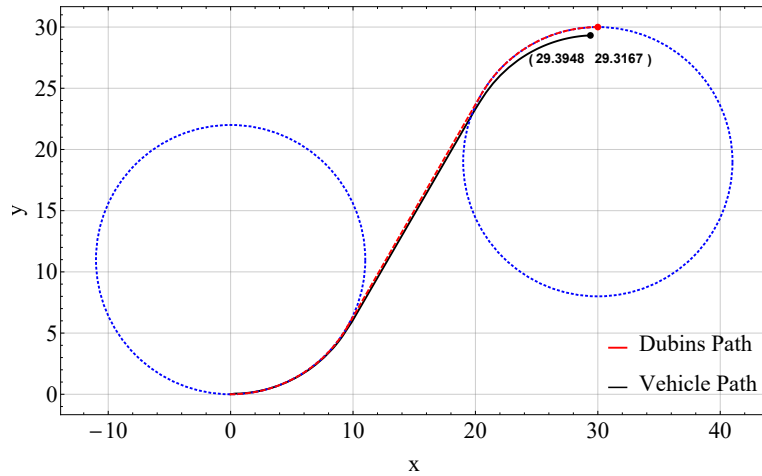


Figure 5.12: The x-y trajectory traversed by the vehicle compared to the actual Dubins path

at the turns can be observed in Fig.5.11 where the rotational velocity increases during the circular sections due to the diameter changes in the system.

Rough Terrain Simulation

To analyze the effects of rough terrain on the vehicle, simulations were done over a period of 50 seconds to study the system's natural response to rough terrain, followed by an attempt to mitigate these effects in open-loop simulations. The aim of this simulation is to attempt bump rejection through the movement of the disk, thus rotational velocity of the disk is kept constant.

The terrain under study consists of a single bump centered at $(15,0)$ with an amplitude of 0.8. This bump is chosen such that one wheel traverses over the center of the bump, while the other wheel is maintained on even terrain.

The effect of this bump on the system is first studied, and the open loop controller is tested to allow the vehicle to traverse rough terrain with minimal effect on its trajectory. Fig. 5.13a shows that the disturbance resulting from the bump is most prominent in the orientation of the system. As the vehicle passes over the bump, the orientation of the system varies resulting in a motion in the direction of the wheel moving over the bump.

To offset this change, the disk is moved towards the wheel that is maintained on even terrain and effectively steers towards it. The deduced change in the disk motion required for bump rejection can be seen in Fig. 5.13b. As a result, the choice of d proves effective in minimizing the net orientation change as seen in Fig. 5.13a. The orientation change is not rejected completely while traversing the bump, due to some oscillation in the disk motion and orientation, but more importantly the trajectory as the system passes the bump is the desired trajectory, observed in Fig. 5.13c.

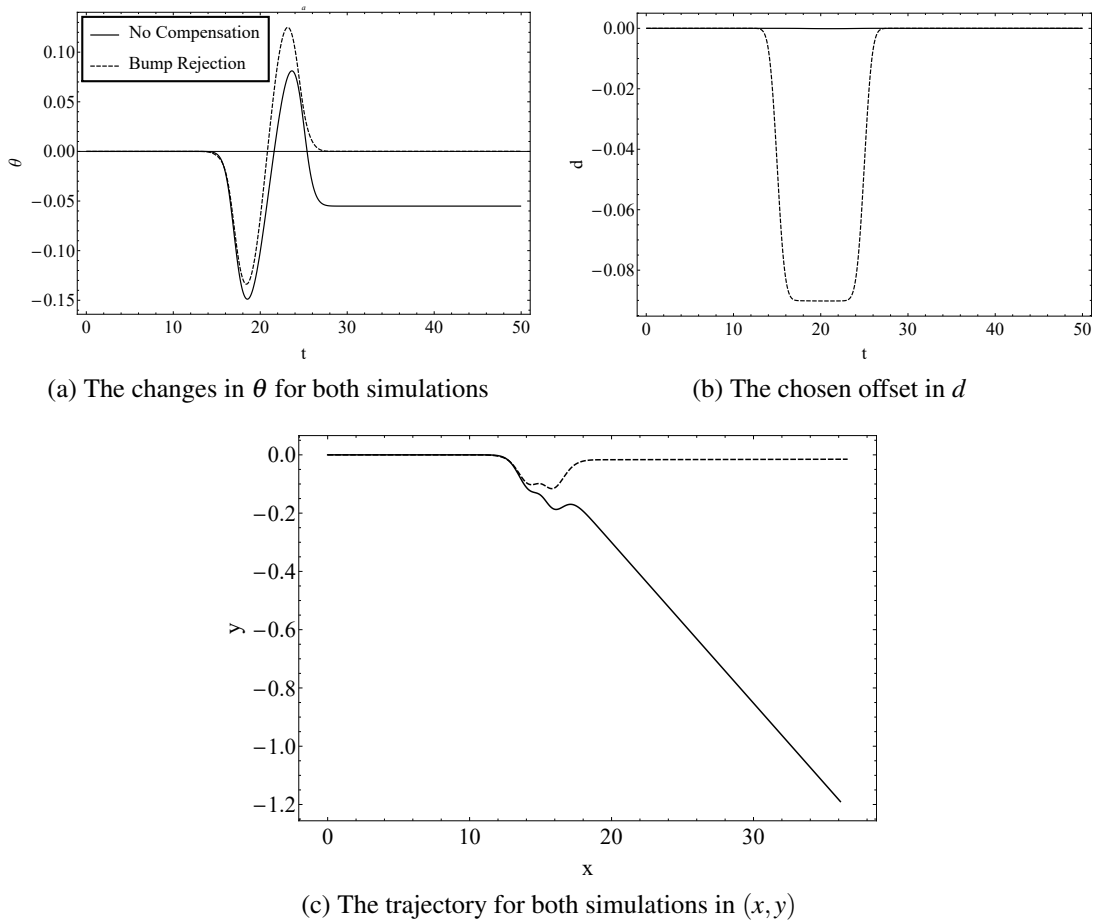


Figure 5.13: Simulation results over rough terrain

The effects of a bump on a system such as this one are on several fronts. A bump is a depiction of added terrain, *i.e.* an added distance for one wheel to traverse. Intuitively, this added distance allows for the wheel on flat terrain to cover more effective ground than the wheel on the bump. Additionally, due to the spring-damper systems modeled in the wheels, the wheel traversing the bump undergoes a diameter increase, as analyzed in previous sections due to a the reduced effect of the ground normal force over the incline, thus the wheel on the bump moves faster than that on flat terrain. A third effect from the bump is the deceleration of the inclined wheel going up the bump as gravitational effects pull it back down, followed by its acceleration as it goes back down the other side of the bump.

As can be seen from Fig. 5.13c, the most dominating effect in this system is due to the added terrain, causing the system to steer towards the bump, and the basic requirement for bump rejection is to offset this net added terrain.

5.3 Simplified Three-Dimensional Model and Control

5.3.1 System Model

In order to implement a controller on the system at hand, a simpler model was developed. Previous simulations have shown the effects of the actuated disk on the system, where the movement of the disk along the wheel axis directly affects its inclination angle, and its rotation about it directly affects the rolling angle of the vehicle. These observations allow for the first simplification being to disregard the disk in order to reduce the set of generalized coordinates by two. A second simplification is a result of basing the model derivation on the center of mass of the system rather than the contact points, such that the position of the center of mass alone is required. Finally, knowing the relationship between the inclination angle and the wheel radii, it is possible to reduce the set of generalized coordinates further by taking the z -coordinate of the center mass and disregarding the radii. These simplifications result in the set of generalized coordinates

$$q = (x, y, z, \theta, \beta, \phi), \quad (5.44)$$

where θ is the orientation of the system in the $x - y$ plane, β is the inclination about the forward direction, and ϕ is the rolling. The center of mass of the system is defined as

$$P = (x, y, z). \quad (5.45)$$

The centers of the wheels can then be defined as

$$\begin{aligned} P_{w,1} &= P + R_{\theta,z} \cdot R_{-\beta,x} \cdot (l, 0, 0), \\ P_{w,2} &= P - R_{\theta,z} \cdot R_{-\beta,x} \cdot (l, 0, 0), \end{aligned} \quad (5.46)$$

where l is half the axis length. The contact points are thus

$$\begin{aligned} P_{c,1} &= P_{w,1} - R_{\theta,z} \cdot R_{-\beta,x} \cdot (0, 0, r_1), \\ P_{c,2} &= P_{w,2} - R_{\theta,z} \cdot R_{-\beta,x} \cdot (0, 0, r_2), \end{aligned} \quad (5.47)$$

where

$$\begin{aligned} r_1 &= \frac{z - l \sin \beta}{\cos \beta}, \\ r_2 &= \frac{z + l \sin \beta}{\cos \beta}. \end{aligned} \quad (5.48)$$

The energy in this system is defined as

$$\begin{aligned} KE &= \frac{1}{2} M \frac{dP}{dt} \cdot \frac{dP}{dt} + \frac{1}{2} m \left(\frac{dP_1}{dt} \cdot \frac{dP_1}{dt} + \frac{dP_2}{dt} \cdot \frac{dP_2}{dt} \right) + \frac{1}{2} m (r_1^2 + r_2^2) \dot{\phi}^2, \\ PE &= \frac{1}{2} k (r_1 - r_i)^2 + \frac{1}{2} k (r_2 - r_i)^2 + Mgz + mg(z_{w,1} + z_{w,2}), \end{aligned} \quad (5.49)$$

where M is the mass concentration at the center of the vehicle, m is mass concentration at the wheels, g is the gravitational constant, k is the spring stiffness, and r_i is the initial radius of the wheels. The Lagrangian is found to be

$$L = KE - PE. \quad (5.50)$$

The constraints on this system are three nonholonomic constraints, two no-slipping constraints on each wheel and a combined no-skidding constraint, such that

$$\begin{aligned} N_1 &= \frac{dP_{c,1}}{dt} \cdot (\cos \theta, \sin \theta, 0) - r_1 \dot{\phi}, \\ N_2 &= \frac{dP_{c,2}}{dt} \cdot (\cos \theta, \sin \theta, 0) - r_2 \dot{\phi}, \\ N_3 &= \frac{dP_{c,1}}{dt} \cdot (-\sin \theta, \cos \theta, 0) + \frac{dP_{c,2}}{dt} \cdot (-\sin \theta, \cos \theta, 0). \end{aligned} \quad (5.51)$$

These constraints are stabilized to give

$$N_{i,s} = \dot{N}_i + \gamma_1 N_i, \quad i = 1, 2, 3. \quad (5.52)$$

The constraint matrix is found to be

$$N_{mat}(i, j) = \frac{dN_{i,s}}{d\ddot{q}_j}. \quad (5.53)$$

such that the constraint forces take the form

$$F_c = N_{mat}^T \cdot \dot{\lambda}, \quad (5.54)$$

where $\lambda = (\lambda_1, \lambda_2, \lambda_3)$ is introduced in a differentiated form for index reduction.

A Rayleigh dissipation function is introduced into the system taking the form

$$D = \frac{1}{2} \mu (\dot{r}_1^2 + \dot{r}_2^2), \quad (5.55)$$

where μ is the damping coefficient. In this system the generalized torques are the ones on β and ϕ such that $\tau = (0, 0, 0, 0, \tau_\beta, \tau_\phi)$. Finally the equations of motion are derived

$$\frac{d}{dt} \frac{\partial L}{\partial \dot{q}_i} - \frac{\partial L}{\partial q_i} - \frac{dD}{dq_i} = \tau_i - F_{c,i}, \quad i = 1, \dots, 6, \quad (5.56)$$

and are appended by the stabilized constraint equations.

Following the process introduced in Chapter 3.2, the equations (5.56) are transformed to take the form of (3.35)

$$\begin{aligned} p &= \dot{q}, \\ \dot{p} &= M(q)^{-1} (\tau + A(q)^T \dot{\lambda} - C(q, p)p - g(q) - b(q)p), \\ \dot{N}(q, p) + \gamma N(q, p) &= 0, \end{aligned} \quad (5.57)$$

where the full state vector consists of $(x, y, z, \theta, \beta, \phi, u, v, w, \Theta, B, \Phi, \lambda_1, \lambda_2, \lambda_3)$. Finally the equations ripe for linearization can be derived from (5.57) providing a system of the form

$$\dot{X} = AX + BU. \quad (5.58)$$

Defining an equilibrium trajectory in (x, y) , it is a simple matter of computing the equilibrium orientation $\theta = \arctan(\frac{y}{x})$. The equilibrium of the states (z, β, ϕ) can be computed using the nonholonomic constraints N_1, N_2 , and N_3 . Finally allowing the computation of λ and the equilibrium inputs using the dynamic equations.

5.3.2 Control and Simulations

Two trajectories are chosen to study the effectiveness of the controller. The first trajectory is a straight line with disturbances providing bump-like dynamics for the simulation. The second is a circular trajectory with the reasoning that if the system can follow both these trajectory, then an optimal Dubins' path is simply a combination of the two.

The system obtained after linearization is not fully state controllable, but in fact only four states are controllable thus requiring a decomposition as seen in Chapter 3.2. Noting that the system is time-varying with equilibrium trajectories(not equilibrium points), this decomposition is performed at every time steps for the total time of the simulation, where the LQR gains are also computed for each time step and introduced into the simulation as time-varying gains.

The parameters chosen for the following simulations are $M = 2, m = 1, l = \frac{1}{2}, g = 10, k = 350, c = 5$, and $r_i = \frac{1}{3}$. It is worth noting the significant stiffness value as to counteract the effect of the weight and maintain a positive z .

Line Following under the Effect of Bump-like Disturbance

For the first set of simulations, the vehicle is made to move along the $x - axis$ with a constant rotational velocity. The initial trial is followed up by adding disturbances on the inclination angle and the height of the system, which is an effect similar to a bump on the road.

The initial trial with no disturbance shows that the controller successfully takes the system to the equilibrium trajectory after the solution converges.

The rotational velocity and inclination angle reach their respective equilibrium values with slight initial deviations as seen in Fig.5.14b and 5.14a, while the motion in the plane shows small error in the y value, in Fig. 5.14c, as the system steers to equilibrium.

For the second simulation, disturbance rejection is studied by adding an impulse on the inclination angle β of magnitude $0.4rad$ at $t = 15sec$. The simulations show the effect of the controller as the disturbance on β is removed, seen in Fig. 5.15b. An important observation is the relationship between the inclination angle and the z

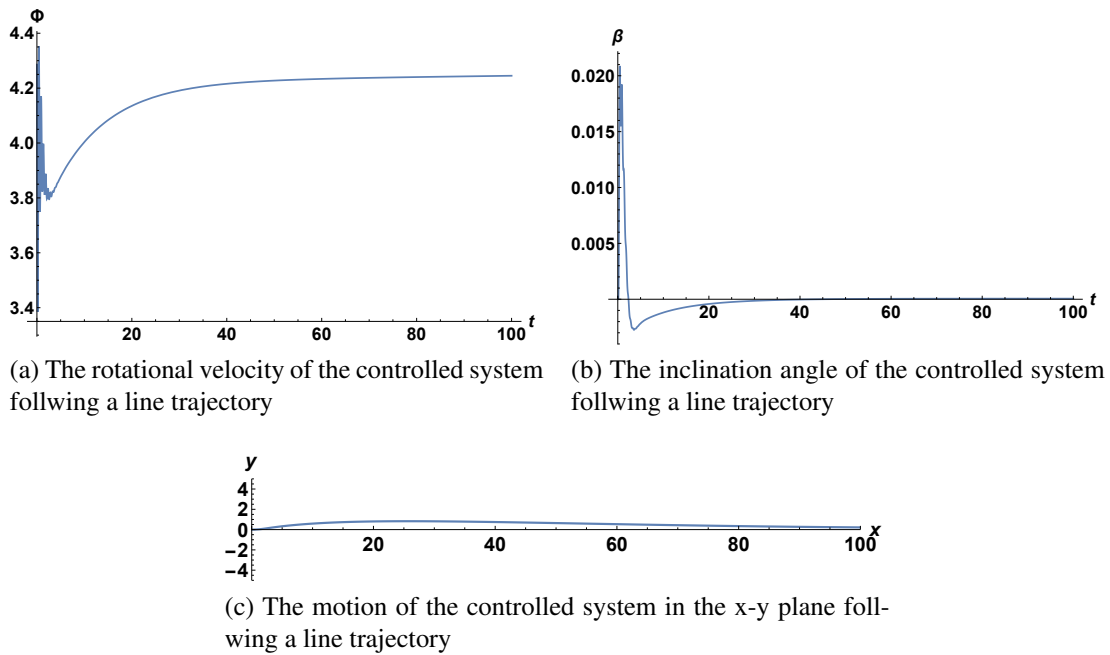


Figure 5.14: Initial simulation result for the controlled system following a line trajectory

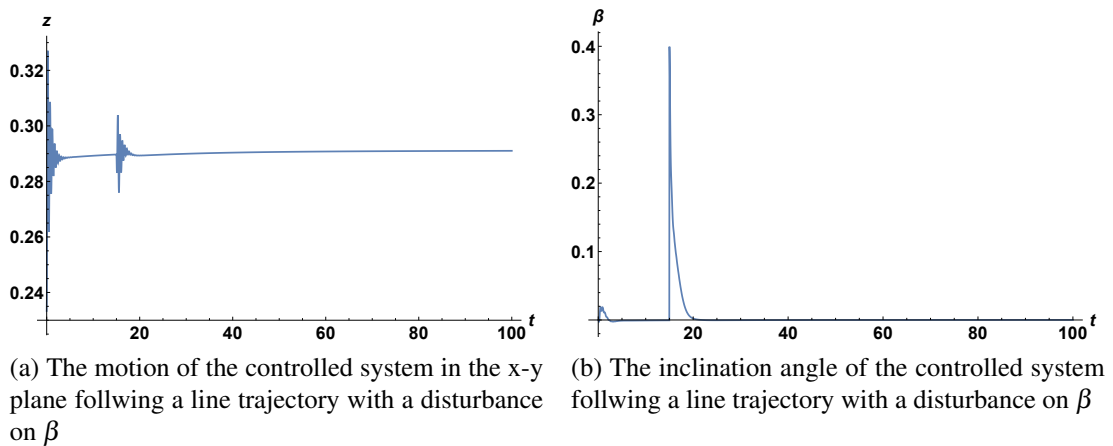


Figure 5.15: The relationship between z and β with a disturbance on β

coordinate of the system, as the disturbance causes a stir in the z coordinate before it settles back to its equilibrium as seen in Fig. 5.15a. The motion of the system in the $x - y$ plane is unperturbed as it remains on its path following the equilibrium trajectory, seen in Fig. 5.16.

For the third simulation, a disturbance on z of magnitude 0.1 is added at $t = 5\text{sec}$. The controller also succeeds on maintaining the system's trajectory by counteracting the disturbance on z as well as that on β as evident from Fig. 5.17a and 5.17b. Noting

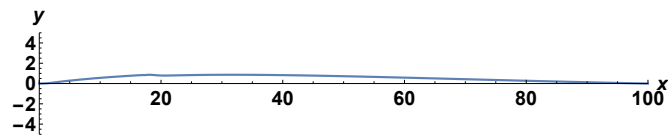


Figure 5.16: The motion of the controlled system in the x-y plane following a line trajectory with a disturbance on β

again that a bump is effectively a combination of increased height and an inclination on the vehicle, these disturbances provide an effect similar to that of a bump on the system. Observing the trajectory tracking in Fig. 5.18 with both disturbances provides a high degree of confidence that this controller has the capabilities to mitigate bumps.

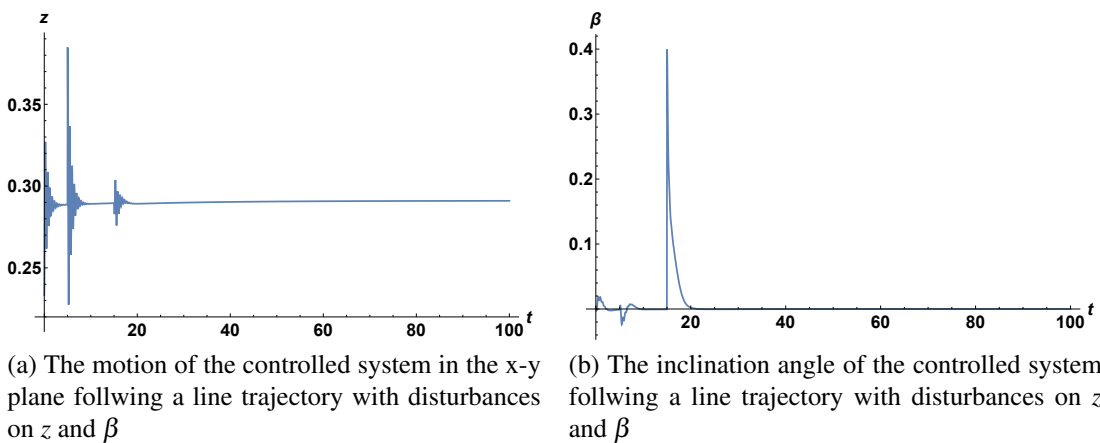


Figure 5.17: The relationship between z and β with disturbances on z and β

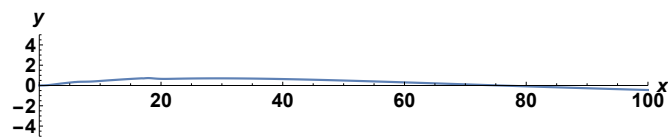


Figure 5.18: The motion of the controlled system in the x-y plane following a line trajectory with disturbances on z and β

Circular Path Following and Robustness

For the second set of simulations, the system is made to follow a circular trajectory with a constant rotational velocity. The initial trial is again followed up by adding a disturbance on the inclination angle of the system, as a study of robustness of the controller.

The initial trial with no disturbance shows that the controller is capable of tracking the circular trajectory within a reasonable error margin. The system undergoes some oscillations to settle into the equilibrium trajectory as evidenced by Fig. 5.19a and 5.19b. These oscillations are a result of several factors, most prominent of which is the presence of a spring-damper in the system. Despite these oscillations, the (x,y) position of the system tracks the original path closely as seen in Fig. 5.19c, which is the main purpose of this controller, and this is a direct result of the choice of the LQR weights.

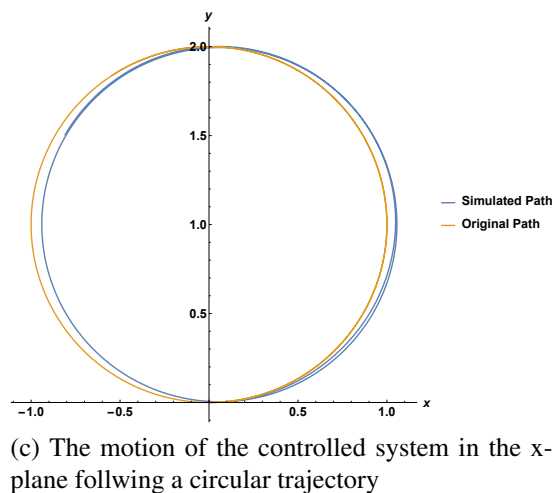
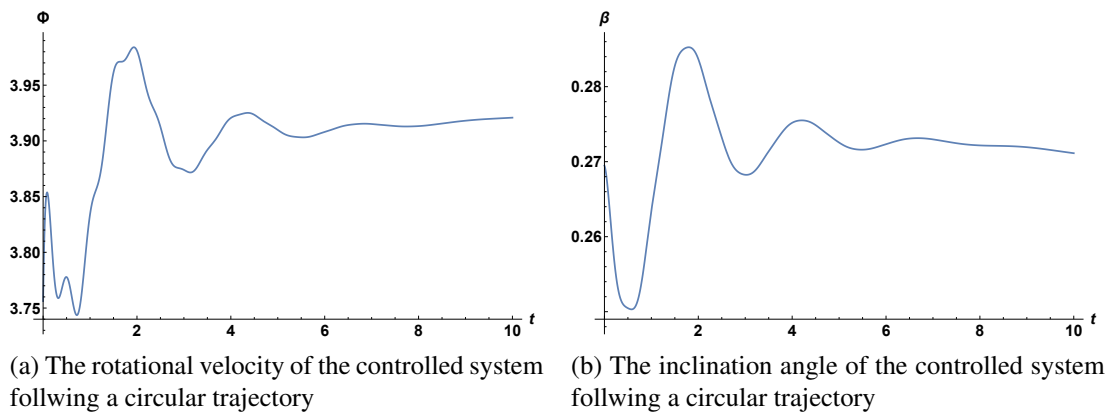
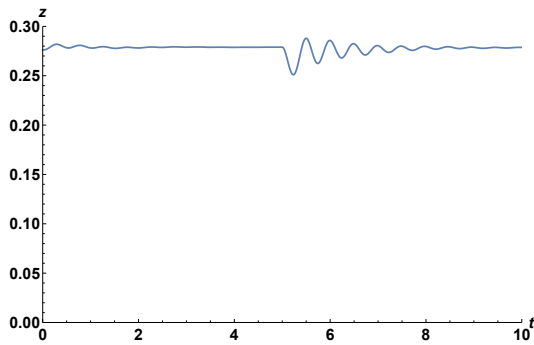


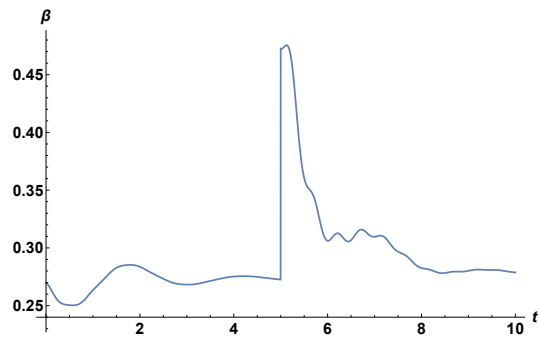
Figure 5.19: Initial simulation result for the controlled system following a circular trajectory

For the second simulation, the robustness of this controller is studied by adding an impulse on the inclination angle β of magnitude $0.2rad$ at $t = 5sec$. This disturbance is again removed by the controller and the system persists in tracking the circular trajectory within a reasonable error margin, observed in Fig. 5.20c. The slight deviation from the trajectory tracking is mainly a repercussion of the nonlinearities in the system and the time steps chosen to solve for the LQR gains. Additionally, this type of

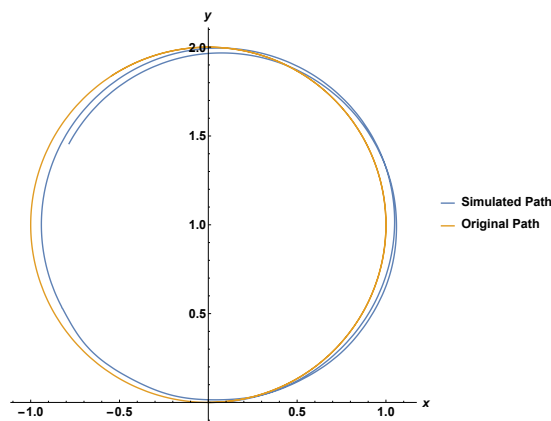
trajectory requires more time for the system to stabilize, as evident in the variation of the z coordinate seen in Fig. 5.20a, where some oscillation occurs before the system reaches its equilibrium z . This is also brought up by the oscillations in β in Fig. 5.20b, where the inclination angle oscillates towards its equilibrium, all a direct effect of the flexible wheels modeled in this thesis.



(a) The variation in the height of the controlled system following a circular trajectory with a disturbance on β



(b) The inclination angle of the controlled system following a circular trajectory with a disturbance on β



(c) The motion of the controlled system in the x - y plane following a circular trajectory with a disturbance on β

Figure 5.20: Simulation result for the controlled system following a circular trajectory with a disturbance on the inclination angle

Chapter 6

Conclusion

This work presented a study on holonomic and nonholonomic robotic systems. As part of this study, a model for a variable diameter differential drive robot was developed and simulated following a Dubins path on flat terrain. Generalizing this model to account for rough terrain mobility proved to be problematic in regards to simulation and modeling.

A novel index reduction technique was then developed based on a constraint stabilization method and the minimum index equivalent of differential algebraic equations. This technique provided an ideal framework to ease the simulation, linearization, and control of high index nonlinear dynamic systems, thus allowing for the expansion of the robotic model to account for rough terrain mobility. Upon studying the effects of rough terrain on a variable diameter wheel, the developed model was used for open loop bump mitigation, where the system was able to follow a desired trajectory under the effects of a bump.

A simplified model was then developed for control purposes, where the developed framework provided the ideal set of equations for linearization and use of linear control. This allowed for the implementation of a linear quadratic regulator on a controllable subsystem of the linearized model. The implemented controller provided a satisfactory response for path following, and a robust response against bump-like disturbances.

Bibliography

- [1] D. OHalloran, A. Wolf, and H. Choset, “Design of a high-impact survivable robot,” *Mechanism and machine theory*, vol. 40, no. 12, pp. 1345–1366, 2005.
- [2] D.-Y. Lee, J.-S. Kim, S.-R. Kim, J.-S. Koh, and K.-J. Cho, “The deformable wheel robot using magic-ball origami structure,” in *Proceedings of the 2013 ASME Design Engineering Technical Conference, Portland, OR*, 2013.
- [3] L. Zheng, P. Zhang, Y. Hu, G. Yu, Z. Song, and J. Zhang, “A novel high adaptability out-door mobile robot with diameter-variable wheels,” in *Information and Automation (ICIA), 2011 IEEE International Conference on*. IEEE, 2011, pp. 169–174.
- [4] D. Hong and D. Laney, “Preliminary design and kinematic analysis of a mobility platform with two actuated spoke wheels,” in *Proceedings of the 2005 IEEE/RSJ Conference on Intelligent Robots and Systems*, 2006.
- [5] J. Sfeir, E. Shamma, and D. Asmar, “Design and modeling of a novel single-actuator differentially driven robot,” in *Advanced Intelligent Mechatronics (AIM), 2014 IEEE/ASME International Conference on*. IEEE, 2014, pp. 1079–1084.
- [6] L. Caracciolo, A. De Luca, and S. Iannitti, “Trajectory tracking control of a four-wheel differentially driven mobile robot,” in *Robotics and Automation, 1999. Proceedings. 1999 IEEE International Conference on*, vol. 4. IEEE, 1999, pp. 2632–2638.
- [7] X. Yun and Y. Yamamoto, “Internal dynamics of a wheeled mobile robot,” in *Intelligent Robots and Systems ’93, IROS’93. Proceedings of the 1993 IEEE/RSJ International Conference on*, vol. 2. IEEE, 1993, pp. 1288–1294.
- [8] P. Abad-Manterola, I. A. Nesnas, and J. W. Burdick, “Motion planning on steep terrain for the tethered axel rover,” in *Robotics and Automation (ICRA), 2011 IEEE International Conference on*. IEEE, 2011, pp. 4188–4195.
- [9] B. Choi and S. Sreenivasan, “Gross motion characteristics of articulated mobile robots with pure rolling capability on smooth uneven surfaces,” *Robotics and Automation, IEEE Transactions on*, vol. 15, no. 2, pp. 340–343, 1999.

- [10] K. Iagnemma, A. Rzepniewski, S. Dubowsky, and P. Schenker, “Control of robotic vehicles with actively articulated suspensions in rough terrain,” *Autonomous Robots*, vol. 14, no. 1, pp. 5–16, 2003.
- [11] J. Baumgarte, “Stabilization of constraints and integrals of motion in dynamical systems,” *Computer methods in applied mechanics and engineering*, vol. 1, no. 1, pp. 1–16, 1972.
- [12] C. S. Cai and B. Roth, “On the planar motion of rigid bodies with point contact,” *Mechanism and Machine Theory*, vol. 21, no. 6, pp. 453–466, 1986.
- [13] C. Cai and B. Roth, “On the spatial motion of a rigid body with point contact,” in *Robotics and Automation. Proceedings. 1987 IEEE International Conference on*, vol. 4. IEEE, 1987, pp. 686–695.
- [14] S. Sreenivasan and P. Nanua, “Kinematic geometry of wheeled vehicle systems,” *Journal of Mechanical Design*, vol. 121, no. 1, pp. 50–56, 1999.
- [15] L. Landau and E. Lifshitz, *Classical mechanics*. Pergamon Press, Oxford, 1960.
- [16] D. T. Greenwood, *Classical dynamics*. Courier Corporation, 1977.
- [17] H. M. Choset, *Principles of robot motion: theory, algorithms, and implementation*. MIT press, 2005.
- [18] K. E. Brenan, S. L. Campbell, and L. R. Petzold, *Numerical solution of initial-value problems in differential-algebraic equations*. Siam, 1996, vol. 14.
- [19] C. W. Gear, “Differential-algebraic equation index transformations,” *SIAM Journal on Scientific and Statistical Computing*, vol. 9, no. 1, pp. 39–47, 1988.
- [20] C. W. Gear, B. Leimkuhler, and G. Gupta, “Automatic integration of euler-lagrange equations with constraints,” *Journal of Computational and Applied Mathematics*, vol. 12, pp. 77–90, 1985.
- [21] M. W. Spong, S. Hutchinson, and M. Vidyasagar, *Robot modeling and control*. Wiley New York, 2006, vol. 3.
- [22] X. Yun and N. Sarkar, “Unified formulation of robotic systems with holonomic and nonholonomic constraints,” *Robotics and Automation, IEEE Transactions on*, vol. 14, no. 4, pp. 640–650, 1998.
- [23] M. C. de Oliveira, *Fundamentals of Linear Control*. preprint, 2015, <http://control.ucsd.edu/mauricio/>. [Online]. Available: ”<http://control.ucsd.edu/mauricio/>”
- [24] C.-T. Chen, *Linear Systems Theory and Design*. Oxford University Press, 1999.

- [25] D. E. Kirk, *Optimal control theory: an introduction*. Courier Corporation, 2012.
- [26] K. Waldron, “Terrain adaptive vehicles,” *Journal of Mechanical Design*, vol. 117, no. B, pp. 107–112, 1995.

